Initiation of Orderly Spinning Detonation Waves via Phased Sparking

Jacob A. Boening

A dissertation

submitted in partial fulfillment of the

requirements for the degree of

Master of Science

University of Washington

2016

Reading Committee:

Carl Knowlen, Chair

Mitsuru Kurosaka

Program Authorized to Offer Degree:

Aeronautics and Astronautics

University of Washington

Abstract

Initiation of Orderly Spinning Detonation Waves via Phased Sparking

Jacob A. Boening

Chair of the Supervisory Committee:
Dr. Carl Knowlen
Aeronautics and Astronautics

A Continuous Rotating Detonation Engine (CRDE) was tested with two unique features. First, the conventional pre-detonator was replaced by a novel detonation wave generator. This generator sequentially fired spark plugs at a speed near the acoustic speed of a reactant gas mixture thereby producing free radicals ready to partake in detonation. The generator produced high speed detonation waves traveling with homogenous direction in gaseous mixtures of H_2 and O_2. Detonation waves continued to spin in a self-sustained fashion after turning off the wave generator. The number of simultaneous sparks did not influence the number of detonation waves observed. Instead the number of observed detonation waves was a strong function of the mass flow rate of reactants. Second, the fuel and oxidizer were injected radially. To avoid the thrust-area loss of conventional axial injection, all injection holes were oriented along the annulus radially, thereby allowing the high pressure to work over the entire front end area. Furthermore, radial injection modulated the mixing of fuel and oxidizer to adjust the axial location of detonation zones avoiding damage to the wave generator.

TABLE OF CONTENTS

LIST OF FIGURES

LIST OF TABLES

ACKNOWLEDGEMENTS

I would like to first acknowledge Carl Knowlen for his guidance and support throughout my graduate education. His expertise in detonation phenomena and detonation experimentation greatly enhanced my contribution to this project. His mentorship and relaxed demeanor made it that much more rewarding and enjoyable to conduct this research under his supervision.

I must also thank Mitsuru Kurosaka for initially bringing me to this research and for his continued receptiveness to my ideas and opinions. I could not have finished this research without his consistent enthusiasm, friendship, and career counseling.

I also thank Tom Mattick for his contributions in the testing phase of this research. As in the design phase, he continued to provide his gracious support of any portions of his electronics system that I managed to incapacitate.

Finally, I thank my wife Betsy for her patience and support throughout my research.

Chapter 1. INTRODUCTION

The Continuous Rotating Detonation Engine (CRDE), sometimes called a Pressure Gain Combustor (PGC), is an advanced and emerging technology. The CRDE could power aircraft and rockets with higher thrust and less fuel consumption by exploiting the thermodynamic advantages of rapid detonation over conventional slower deflagration [1]. Contrary to the so-called pulsed detonation engine (PDE), which provides thrust intermittently, the CRDE can truly deliver continuous thrust. This paper presents the unique design and successful testing of a 6-inch-diameter CRDE at the University of Washington. Before presenting details of the UW design, a brief description of detonation, its importance in propulsion, present status and problems will be described next.

1.1 DETONATION

Detonation is a combustion-driven shock wave typically propagating at the Mach number range of 5-10. The fast moving shock ingests fuel and oxidizer ahead of the wave and compresses them to higher pressure. This compression, combined with the temperature rise across the shock, results in rapid chemical reaction, which provides the energy necessary to self-sustain the forward propagation of the shock. The chemical reaction acts like a piston driving a shock as shown in Figure 1.1. In deflagration, the more common mode of burning used in the internal combustion engine or conventional gas turbine burner, the chemical reaction proceeds at slower rate, with a maximum flame speed of less than Mach 0.03.

Figure 1.1. Detonation wave with shock and reaction zone immediately behind the shock (yellow/orange) [3].

Ahead of the shock of Figure 1.1, the fuel and oxidizer are either at rest (for PDE) or flowing perpendicular to the paper (CRDE): there is no significant propellant motion in the direction of shock motion. Behind the moving shock, static pressure rises and gas behind follows the footsteps of the propagating shock. As a result, total or stagnation pressure increases more than tenfold by

detonation. It is for this reason that CRDE is classed as a PGC. This is in contrast to deflagration where the total pressure always decreases. Total pressure is one of the determinants of thrust; the higher the total pressure, the larger the thrust. This is one of the advantages of the CRDE for high speed propulsion.

Temperature-entropy diagrams for three cycles: the Brayton cycle for gas turbines, the Humphrey or constant-volume cycle, and the detonation engine (DE) cycle are shown in Figure 1.2. The key point to note is that the DE cycle operates at the highest temperature, which results in minimum entropy increase among the three. Regardless of the cycle, the entropy increase must end up as heat rejection to the ambient air. Thus the CRDE/PGC can achieve higher efficiency and generates power with less greenhouse gas emission.

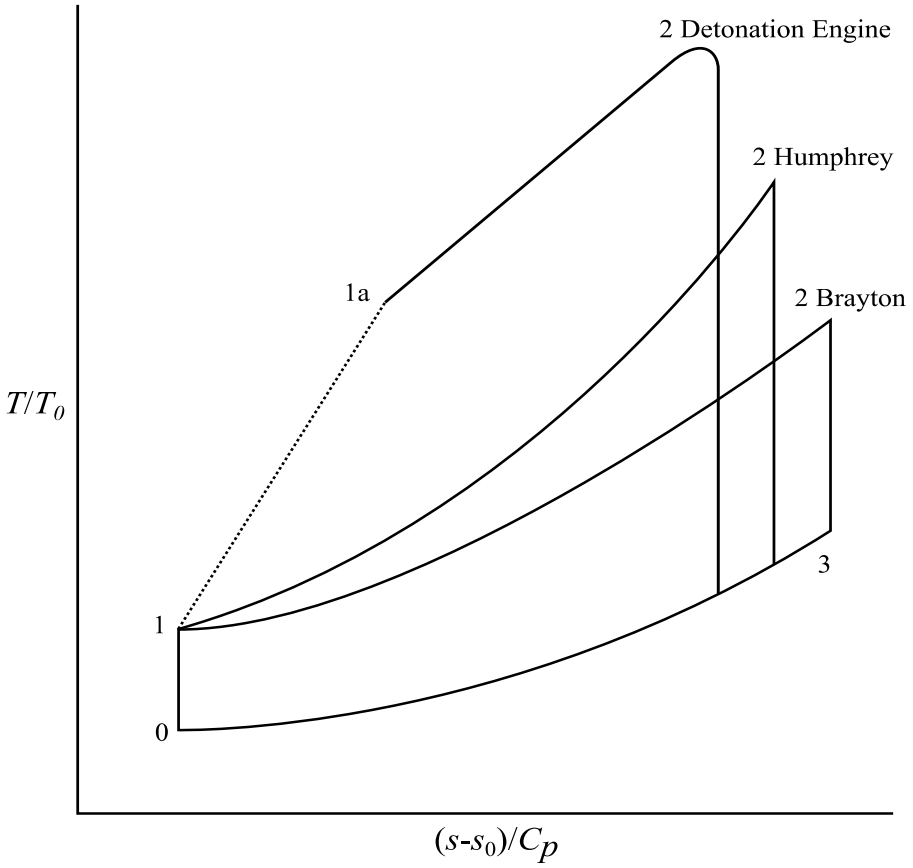

Figure 1.2. T-S diagram of DE, Humphrey, and Brayton cycles [4].

1.2 OPERATION

The CRDE uses an annular combustion chamber to enclose detonation waves which travel azimuthally. Fuel and oxidizer are constantly injected into one end of the combustor. The detonation wave consumes the reactants as it rotates around the annulus. Provided that the combustion reactants are continuously injected, the detonation wave is self-sustaining. A depiction of this process is shown below in Figure 1.3.

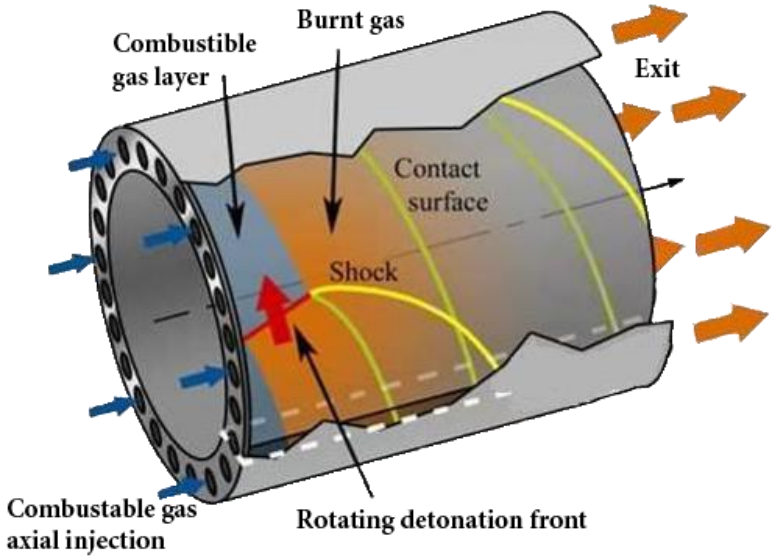

Figure 1.3. Continuous rotating detonation operation in an annulus.

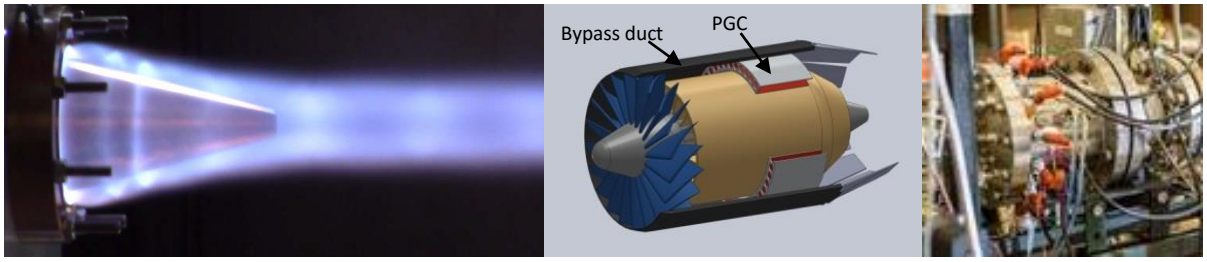

(a) (b) (c)

Figure 1.4. (a) GHKN PGC in rocket mode [5], (b) PGC in bypass-duct mode, (c) UW CRDE.

Figure 1.4a shows the use of a PGC in a rocket configuration, which provides additional advantages for non-toxic storable green propellants [5]. The installation of a CRDE/PGC in the bypass duct of a gas turbine is shown in Figure 1.4b. The resulting total pressure gain can increase

the bypass thrust by more than 30% and can eliminate the afterburner in supersonic flight. Despite these potential applications, the CRDE is still in a nascent developmental stage [5]-[15].

1.3 Features: Detonation Wave Initiation and Mixing

One of the challenging issues facing CRDE development is the wave directional instability. A detonation wave is commonly initiated using a pre-detonator. This device, shown in Figure 1.5, is aligned tangentially to the combustor, and a detonation wave is 'shot' into the annulus. Despite the intent for the pre-detonator to generate waves spinning in one direction, it has been reported that once the pre-detonator waves enter the annulus, two counter-rotating waves are observed in the annulus; when they collide, the result is unstable operation and, in the worst case, termination. Instead of this inadequate one-shot pre-detonator, the UW design features a spinning wave generator, which can initiate waves spinning in the preferred circumferential direction by progressive azimuthal provision of spark energy.

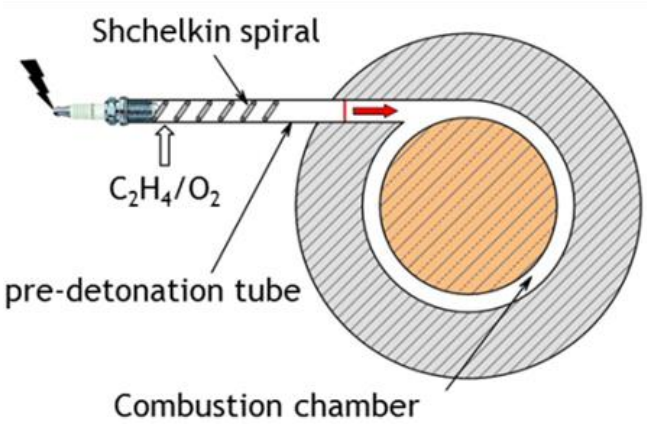

Figure 1.5. Pre-detonator as installed in a CRDE [6].

Another feature of the UW design utilizes radial counter-flow injection of fuel/oxidizer. In the axial injection used by others (Figure 1.3), where there are multiple holes on the front end plate, the pressure gained by detonation cannot fully be utilized to push the end plate. In contrast, in the radial injection, the plate in its entirety can take the full brunt of pressure gain for forward thrust.

Chapter 2. ENGINE DEVELOPMENT AND DESIGN

The primary design goal of this CRDE was to implement the novel detonation wave generator concept. My group also recognized that it would be beneficial to delay mixing to an axial location downstream of the wave generator so that detonation combustion products did not come in the vicinity of the wave generating spark sources. The wave generator concept is introduced here first followed by an explanation of the operation of the modulated mixing.

2.1 WAVE GENERATOR

The most important element of the CRDE is the system designed to initiate the detonation waves. This system is called the wave generator. The theory behind the controller involves generating sequential shock waves or blast waves with phasing at varying azimuthal locations on the annulus. Owing to the non-linear aspect of the path of the waves, the combined waves will coalesce to form a strong single wave. The curvature of the annulus forces the wave to travel circumferentially. This phenomenon is called the whispering gallery effect. The name stems from a specific scenario involving a large amphitheater style building, a gallery, that has a continuous circular wall with a large diameter. If a person standing very close to the wall were to whisper in a tangential direction, another person on the opposite half of the circle would still be able to hear the whisper despite being a significantly long distance apart.

There are several famous buildings that exemplify this phenomenon, one being St. Paul's Cathedral in London. Even though the annular duct of the combustor is significantly smaller in diameter when compared to a large gallery, the principle still applies. While the whispering gallery effect is helpful in sustaining the pressure wave, the wave will eventually damp out. This is because the strength or intensity of a pressure wave is inversely proportional to the square of the distance, hence the need for sustaining the original wave generated by the spark. Therefore, an initial blast wave that is consistently sustained by successive blast waves would create a single transverse wave that would rotate around the annulus at a prescribed velocity.

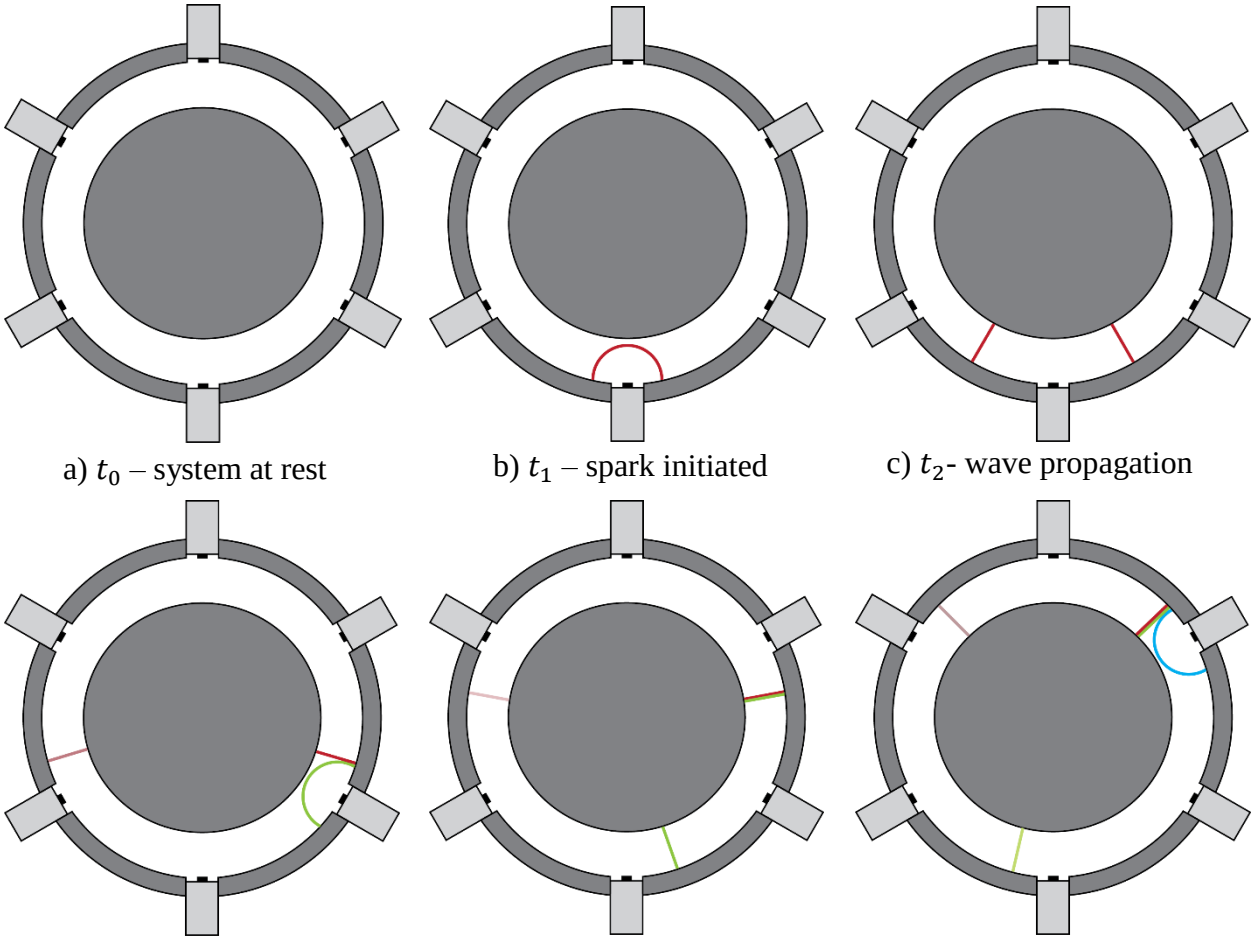

a) t_0 – system at rest b) t_1 – spark initiated c) t_2- wave propagation

d) t_3 – second spark fired e) t_4 – wave propagation f) t_5 – third spark fired

Figure 2.1. Schematic of sparking for wave generator. Each color represents a new wave from a spark plug.

A single blast wave can be initiated quite simply with a standard spark plug. While a spark plug typically acts as a catalyst to initiate a combustion reaction, the spark also creates a spherical blast wave emanating from the electrode location. From geometry constraints, the best location for the spark plug is along the exterior of the outer cylinder of the annulus, with the spark itself being perfectly tangent to annular duct wall. Due to the blast wave's hemispherical nature, a wave emitted from the outer interior wall of the annulus will travel in both azimuthal directions as well as axially. This presents a problem since the eventual goal is to generate a single detonation wave traveling in one direction. By adding more spark plugs around the exterior of the annulus at the same axial position, the wave can be encouraged to travel in one azimuthal direction. This is done by timing the blast waves in such a way that successive waves would be perfectly tuned to each

other, thus generating a coalesced transverse shock wave. The tuning process for the blast waves is conceptualized above in Figure 2.1.

In the first frame of the figure, a 2D cross-sectional view of the annular duct is shown. The 6 equally spaced rectangles represent the spark plugs or blast wave generators. The next frame depicts a moment slightly after the first spark plug is fired. Due to the 2D simplification, the blast wave is illustrated as a red circular arc. As time marches forward, the blast wave continues down both sides of the annulus at a velocity slightly above the speed of sound. Once this wave reaches the next two adjacent spark plugs, only one fires. Thus one azimuthal direction of the initial wave is amplified and the other segment eventually decays. This is illustrated by Figure 2.1b-f. With the initial wave strengthened, the next spark plug further magnifies the intensity of the wave. By continuing to bolster the wave with additional sparks at the appropriate time intervals, a transverse wave will emerge in less than a millisecond. Sparks also create successive pools of free radicals in the circumferential direction, which prompt chemical chain reaction, and the spinning transverse waves will transit into spinning detonation waves. This activity of this spinning wave generation is shown in the shadowgraph image of Figure 2.2. The image was taken in an open-ended version of the CRDE which permitted the shadowgraph technique.

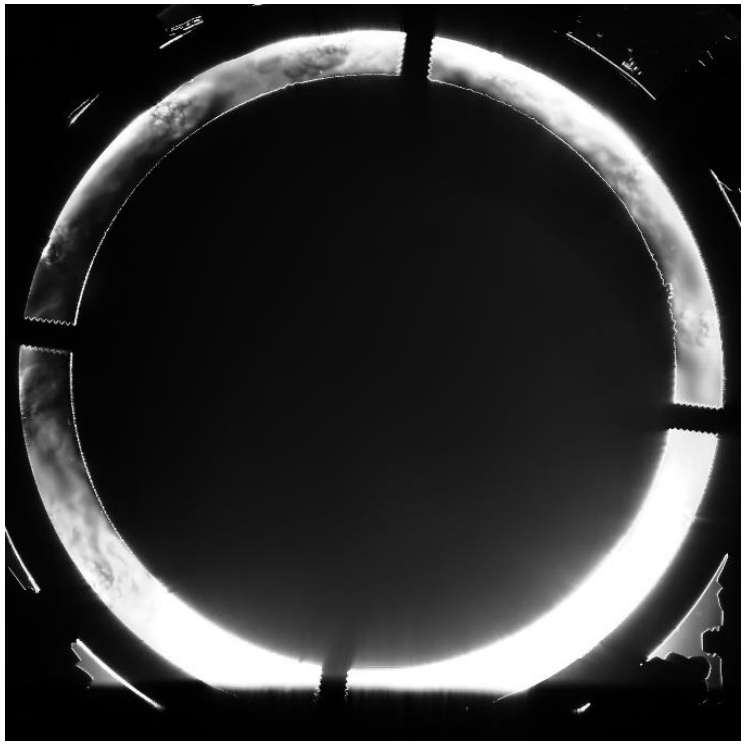

Figure 2.2. Shadowgraph of wave generator in a mock-up version of the CRDE during operation.

Detonation initiation involves the combustion of a fuel and oxidizer in combination with a mechanism to induce acceleration of the combustion front in a manner that generates a shock wave. The transverse wave created by the spark plugs acts as the mechanism to transform the combustion from deflagration to detonation. Not only do the spark plugs create the rotating wave, they also ignite the fuel and oxidizer when both are introduced into the annulus. Once the detonation wave is indeed created, there is no need to control its motion in the annulus via the spark plugs because the detonation wave is self-sustaining. This requires that the detonation wave be continuously supplied with well-mixed fuel and oxidizer. If for some reason the detonation wave begins to migrate in the opposite direction from its original course (which has happened in other continuous rotating detonation research), the wave generator can help compensate for the deviation and maintain smooth operation.

Transferring the 2D conceptual design of the wave generator depicted in Figure 2.1 into three dimensions resulted in the design illustrated in Figure 2.3. As shown in this figure, the final design increased the number of spark plugs from six to twelve. This allowed for more modes of operation since it can now generate up to four waves simultaneously. Also, by using twelve spark plugs, the distance for a blast wave to travel before it is enhanced was decreased. This increases the overall energy input to the system by the spark plugs, but also enhances the ability of the wave generator.

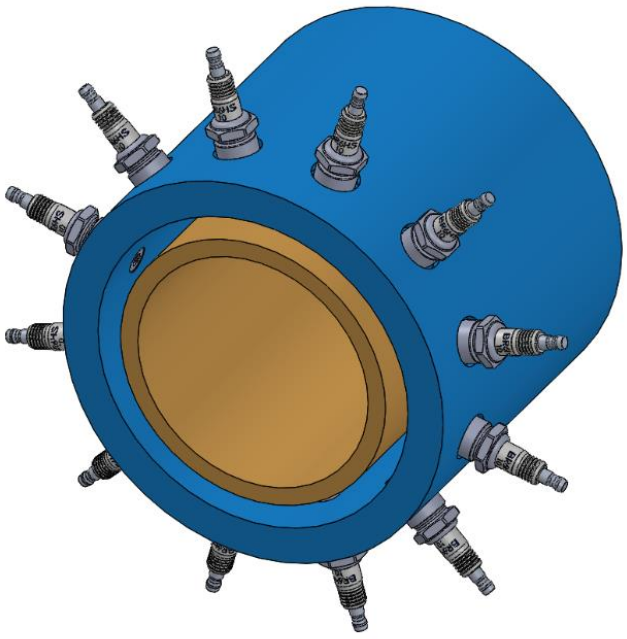

Figure 2.3. Spark plug array azimuthally aligned at a single axial location.

The electronics behind the spark plug firing mechanism are explained in a general manner. The main component of the spark plug mechanism is the wave controller box. This box required the input of a function generator and a variable power supply with the ability to control the amperage and voltage. The wave controller box would then output 12 signals; one to each of the spark plugs. Figure 2.4 below illustrates this general electrical schematic.

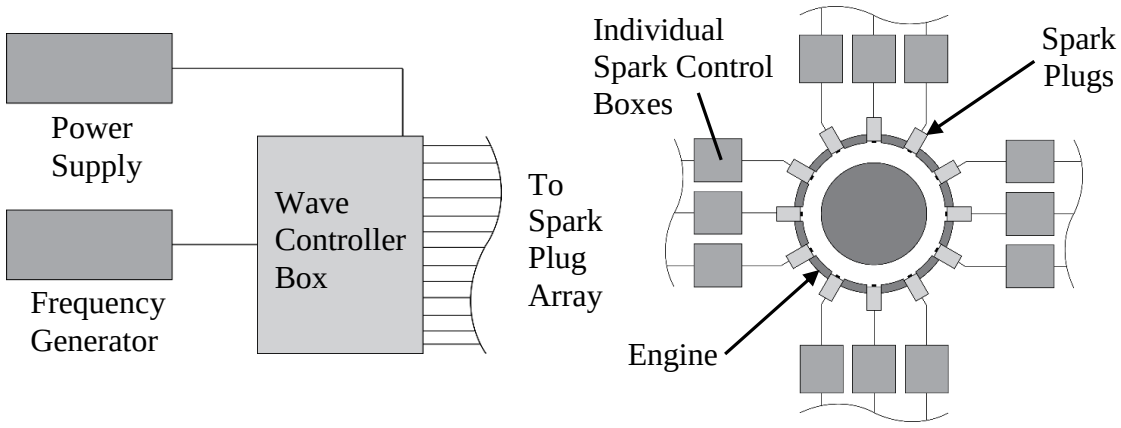

Figure 2.4. General schematic for the spark plug electronics.

The wave controller itself had the ability to set the number of waves generated by the spark plug array. It was capable of creating from 1 to 4 distinct waves. The function generator was used to set the frequency of the waves. The function generator frequency corresponded to 12 times the frequency of an individual spark plug.

The particular frequency used in operation corresponded to the time required for a single acoustic wave to make one full rotation around the annulus when the gaseous medium is air. This is also known as the speed of sound frequency. The equations to obtain these values for n-number of waves are given below.

$$f_{\text{input}} = 12 f_{\text{spark}} \tag{2.1}$$

$$f_{\text{spark}} = n_s V/(\pi d_c) \tag{2.2}$$

$$a = \sqrt{\gamma RT} \tag{2.3}$$

$$f_{\text{spark}} = n_s \sqrt{\gamma RT}/(\pi d_c) \tag{2.4}$$

In these equations, f is the frequency, d_c is the mean diameter of the annulus, n_s is the number of simultaneous waves generated by sparks, V is the velocity of a wave, a is the speed of sound for the specific gas, γ is the ratio of specific heats for the gas, R is the specific gas constant, and T is the temperature of the gas.

2.2 MODULATED MIXER

Rather than axially drilling injection holes through the front-end plate, it is desirable to leave the front-end surface unperforated so that its entire surface can fully take thrust producing pressure. Thus in contrast to designs using axial injection, in the UW CRDE, our group adopted radial injection. The fuel and oxidizer are injected radially from outer and inner walls and in circumferentially staggered manner to induce counter-rotating vortices which mix them by entrainment as in Figure 2.5. By the use of sparse number of holes, it is found that the mixing can be modulated in such a way that the detonation zone can be axially delayed to separate the detonation from the wave generator.

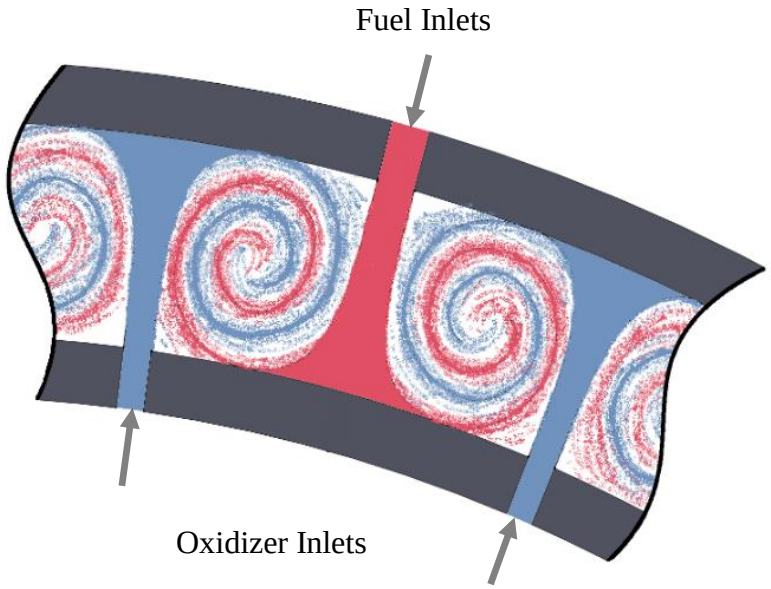

Figure 2.5. 2D illustration of coaxial vortices developed from perfectly offset radial injection.

Chapter 3. EXPERIMENT SETUP

The performance characteristics of two devices, the wave generator and modulated mixer, were examined using one test facility which did not change substantially depending on which of those two devices was examined. This chapter describes the setup of that facility and various issues encountered with the setup.

3.1 CRDE DESIGN

The design of the UW CRDE is covered extensively by Heath [16]. For easy reference, a summary of key dimensions is provided in Table 3.1. An overall view of the CAD model of the engine is provided in Figure 3.2. A cutaway view giving an idea of the gas flow path is shown in Figure 3.3.

Table 3.1. CRDE primary dimensions summary.

Dimension	Value
Centerline Diameter	14.28 cm
Annular Gap Height	1.12 cm
Exterior Wall Thickness	1.75 cm
Interior Wall Thickness	0.86 cm
Combustor Length (measured from spark plug array)	13.97 cm
Fuel Injection Hole Diameter	1.19 mm
Oxidizer Injection Hole Diameter	1.78 mm
Number of Fuel Injection Holes	12
Number of Oxidizer Injection Holes	12

In order to keep parts from protruding into the flow induced by the detonation wave, button-style NGK BUHW-2 spark plugs were used. These do not have a hook-style electrode, but instead have a center-post electrode that sparks across the annular gap between electrodes. The exact orientation of the spark across the face of the plug is allowed to spontaneously change during operation and does not significantly impact performance. A side-profile photo and CAD rendering of the plug can be seen in Figure 3.1 and Figure 3.3.

Figure 3.1. Profile view of button-style spark plug.

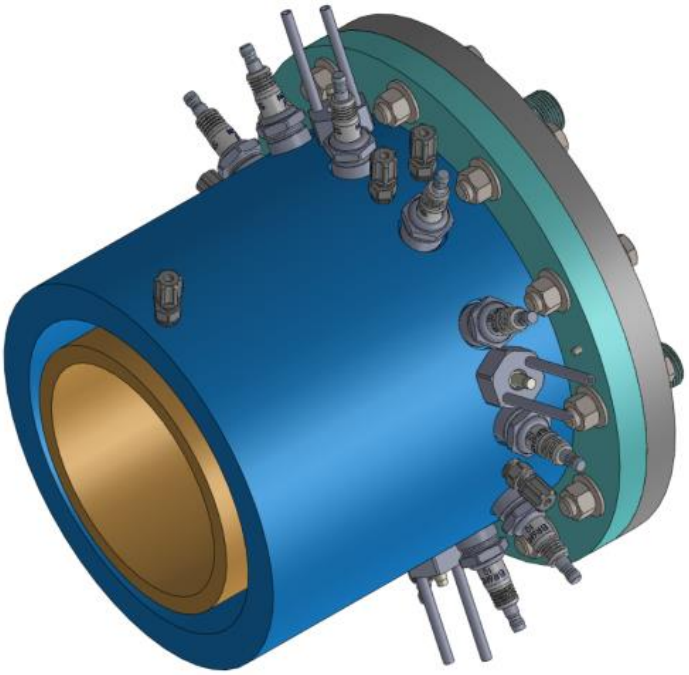

Figure 3.2. Overall view of UW CRDE.

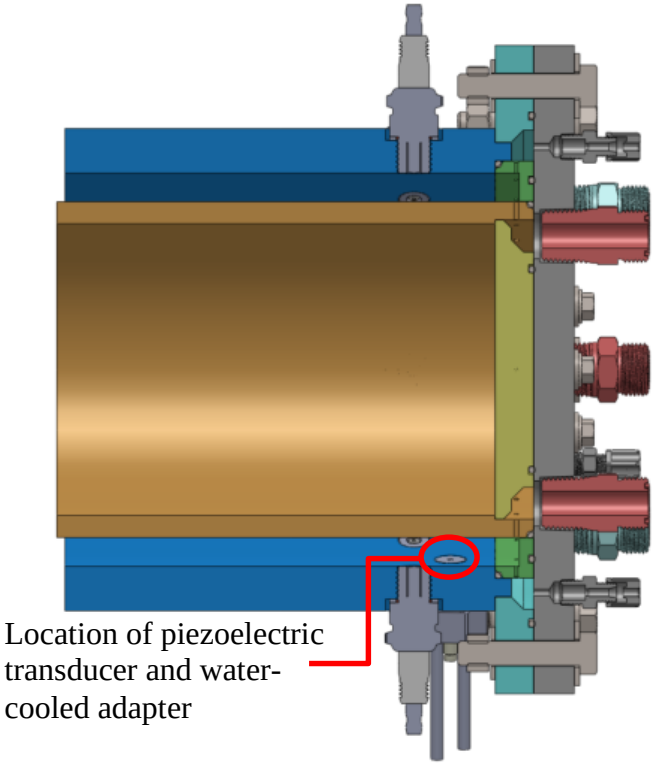

Figure 3.3. Cutaway view of UW CRDE.

3.2 GAS HANDLING AND DIAGNOSTICS

Because the combustor was designed for use in the SWR, much of the gas handling system was already in place at the start of the experiment setup. The schematic in Figure 3.4 illustrates the gas handling system in its entirety.

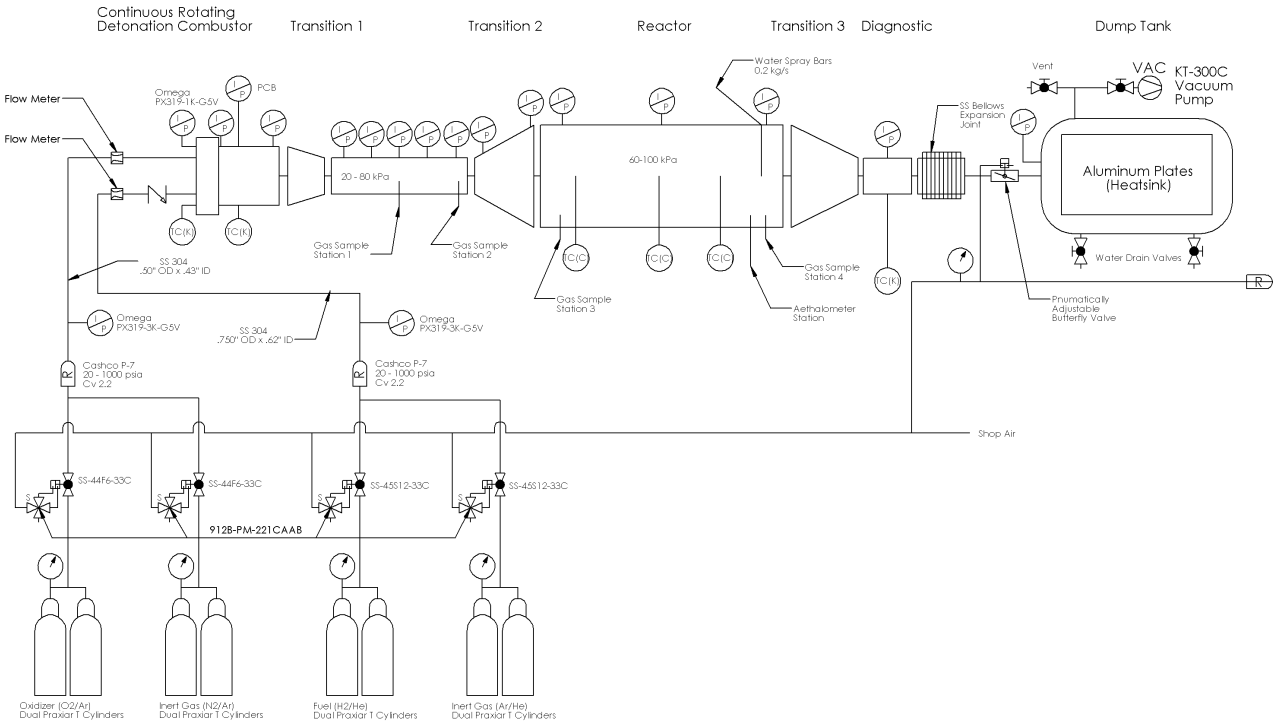

Figure 3.4. Schematic of the gas handling system for the CRDE.

Commercial gas cylinders pressurized anywhere from 300-2600 psi provided the source of the fuel, oxidizer, and inert purge gases during the experiment. The regulators attached to these cylinders were set in the range of 100-200 psi so that, considering pressure drop in the lines to the regulators, the pressure regulator behaved erratically below a cylinder pressure of about 300 psi.

For the first runs of the experiment, argon and helium were used as the purge gases because they generated a mixture with a similar sound speed to a mixture of oxygen and hydrogen. Matching the purge and inert sound speeds seemed important so that a shock wave of similar speed was generated before the introduction of a reactive mixture, in effect skipping any deflagration burning step that might occur if the wave generator had tried to directly ignite the reactive mixture. This phenomenon was never observed, and in fact, the wave generator detonated the mixture with no

pre-purge gas whatsoever on several occasions. The inert pre-purge gases were then replaced with nitrogen in light of its lower cost. Nitrogen was used as the inert gas throughout the rest of the experiment.

Inert gas lines connected into both the fuel and oxidizer lines for easy transition between reactive and inert gas. The fuel and oxidizer each passed through a flow regulator set to the desired pressure. They then passed through a Venturi style flow meter which measured the flow rate. After the flow meters, the oxygen and hydrogen flows split into four lines each and entered their respective manifolds. The pressure in these manifolds controlled the flow rate of gas to the system. A valve was connected to the hydrogen line enabling the release of any hydrogen leftover in the line to the roof of the building for safety reasons. After combustion in the annulus, the exhaust traveled down a 4-m-long stretch of pipe sections (10-cm and 25-cm-ID) and finally into an evacuated dump tank.

The data acquisition system sampled static pressure measurements of the flow at a rate of 2 kHz at several points throughout the system. These points included the gas cylinders, Venturi meter freestream and throat locations, H_2 and O_2 manifolds, various locations along the annulus of the CRDE (combustor pressures), and various locations in the mixer, transition, and reactor sections downstream of the CRDE. Additionally, the DAQ sampled two high frequency response PCB® piezoelectric pressure transducers at a rate of 1.25 MHz in order to capture high speed detonation phenomena. The piezoelectric transducers were installed in PCB® 064B06 water-cooled adapters to maximize transducer life and minimize drift in the signal due to warming of the piezoelectric components. The water-cooling adapter also acted as a snubber, with only a small hole at the end of the jacket attenuating the pressure and temperature associated with the detonation wave. With this setup, none of our piezoelectric transducers ever failed.

Table 3.2. Model information for sensors vital to determining wave behavior

Sensor	Manufacturer	Model
High frequency pressure transducers	PCB®	112-A05, 113-B22
Manifold pressures	Omegadyne®	PX319-1KG5V
Venturi meter pressures	Omegadyne®	PX319-500G5V
Combustor pressures	Omegadyne®	PX319-500G5V

The axial and azimuthal locations of the transducers in the CRDE's outer shell were varied throughout testing. One representative location is visible in the CAD model of Figure 3.3. The remaining locations are represented in Figure 3.5 in which the letters A-M provide unique

identifiers to each position and the numerical value after each letter indicates the distance downstream of the spark plug axial position (if upstream the value is negative). The figure shows the orientation of the CRDE relative to the lab and uses one line to represent a possible transducer location.

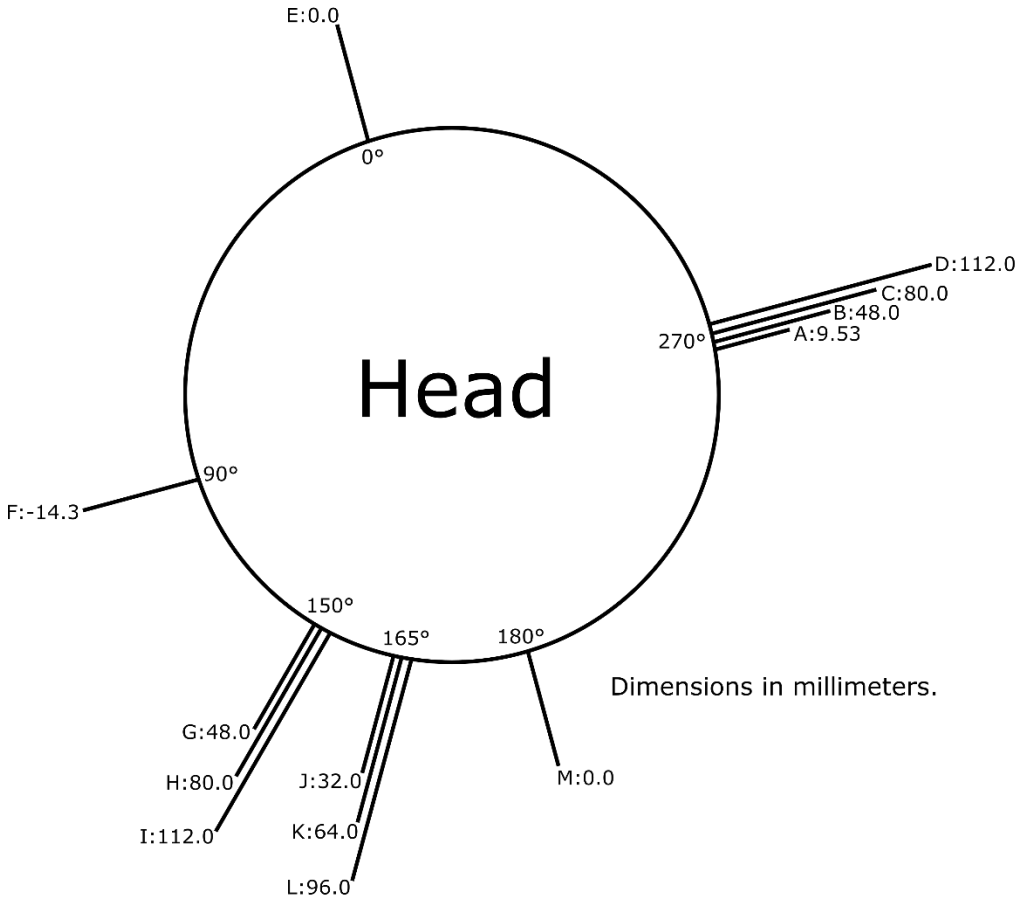

Figure 3.5. Possible locations for piezoelectric pressure transducers.

Two primary location configurations were used. The first configuration had one transducer at A and the second transducer at E. This configuration provided general wave speed data, and did not detect variation in the axial direction. This is desirable for the time of flight analysis method described in Chapter 4. If both transducers were detecting the same part of the detonation wave, then the arrival times could reliably be compared. The second configuration had one transducer at E and the second transducer at G. This configuration was used to detect variation of wave intensity in the axial direction as well as in the azimuthal direction. The purpose of this configuration was to detect the axial length of the detonation wave, but it was ultimately too difficult to axially locate the wave to make this configuration effective.

3.3 TEST PROGRAM

Experiments with the CRDE were conducted according to the following sequential procedure.

1. The system was evacuated to less than 5 kPa while the isolation valves were closed.
2. A pre-run checklist (Appendix A) was followed to ensure all experiment subsystems were operational.
3. A safety switch was enabled allowing communication between the control system and the solenoid-operated isolation valves.
4. The remote, high-speed LabVIEW VI was armed and the run was started from the local LabVIEW VI.
5. The DAS recorded baseline sensor data for 1 second.
6. The controller opened the N_2 isolation valve to allow an inert gas pre-purge to flow for approximately 1 second.
7. After pre-purge, the controller started the spark generator, and, within 100 ms, H_2 and O_2 isolation valves were opened to allow reactive flow into the combustor.
8. After ignition, usually within 100-300 ms of opening the reactive flow isolation valves, the controller turned off the spark generator.
9. The controller allowed the engine to run in a self-sustained fashion for the remainder of one total second of reactive flow.
10. The controller closed the reactive flow isolation valves and opened the inert gas isolation valves to initiate a 1 second, inert gas, post-purge of N_2.
11. If no ignition was observed, then the system contents were immediately exhausted through a line leading to the outside of the building.

The experiment operated at variable total mass flow rates of 20-200 g/s, while the fuel-oxidizer equivalence ratio was varied between 0.5 and 2. The pressure regulator settings were held constant during a run, so fluctuations in the flow rate and equivalence ratio during a run were due to transient behavior in the regulator mechanisms. The frequency generator operated between 14.4 kHz and 28.8 kHz producing individual spark plug frequencies of 1.2 – 2.4 kHz. The number of simultaneous sparks varied from 1 to 4. A butterfly valve downstream of the test section controlled the back pressure. It was varied from approximately 10° (nearly closed) to 90° (fully open). The

above test procedure was run for many values within these ranges. The results of those runs are presented in Chapter 5.

3.4 MASS FLOW RATE CORRECTION

After approximately the 150th test, the venturi flow meters were found to be incorrectly calibrated or outside their measurement range so that recorded mass flow rate measurements were incorrect. After this point, the pressure gauges which measured freestream and throat pressure of the venturi meters were replaced with gauges which have appropriate range and were able to record absolute pressure as opposed to pressure differential, and the incompressible mass flow rate calculation of Equation 3.1 was altered to include compressible effects.

The incompressible Venturi flow rate calculation

$$\dot{m} = C_d A_2 \sqrt{\frac{2\rho(p_2 - p_1)}{1-\beta^4}} \tag{3.1}$$

where $\beta = \frac{d}{D}$ becomes

$$\dot{m} = C_d A_2 \sqrt{\frac{\left[p_1 \rho_1 \frac{2\gamma}{\gamma - 1}\right]\left[\left(\frac{p_2}{p_1}\right)^{2/\gamma} - \left(\frac{p_2}{p_1}\right)^{1+1/\gamma}\right]}{1-\beta^4\left(\frac{p_2}{p_1}\right)^{2/\gamma}}} \tag{3.2}$$

In order to still make use of the data from the first 150 runs, I correlated by linear regression the manifold pressure with mass flow rate from runs with known good mass flow rate data. I then applied the correlation to the manifold pressures from the first 150 runs to determine the correct mass flow rates for those runs. This process was relatively straightforward and produced the linear correlation of. The only difficulty lay in that the manifold pressures and mass flow rates are averages and I needed to determine the averaging period for each run from their plots by visual inspection to ensure I took averages only over steady flow periods.

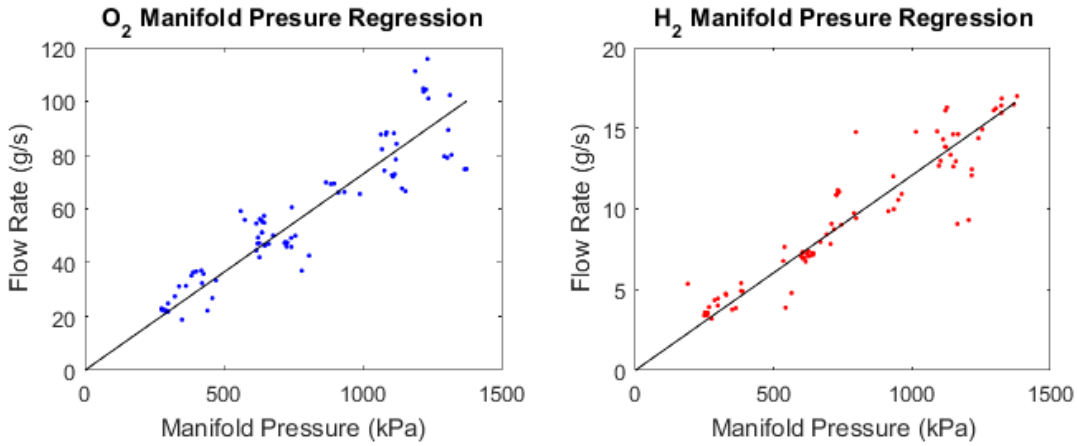

Figure 3.6. Plots of the regressions used to correct prior run data.

3.5 Intermittent Sparking

Initially I intended to integrate the frequency generation for the wave controller into the LabVIEW VI that I used for controlling the valve sequencing and data acquisition. This seemed to work initially, but later I found this difficult to configure correctly. In fact, I found that high frequency signals were occasionally being generated and sent to the wave controller, causing spark plugs to fire. If a run did not ignite, leaving a reactive mixture present in the system, it was undesirable that the sparks should fire between the end of the run and the pumping of the mixture to the roof. However, sparks did intermittently fire, occasionally leading to untimely ignition either immediately after the run or while an assistant or I were near the rig. Because of this unsafe sparking behavior, the LabVIEW generator was removed in favor of a simple switch that controlled whether the output of an independent frequency generator reached the input of the wave controller. I had no problems with intermittent sparking after this modification.

3.6 Burn Marks & Flame Holding

After performing over 100 runs with the CRDE, I removed it from the test configuration to physically inspect its condition. I observed some charring of the interior annulus surfaces and interior pressure manifold surfaces.

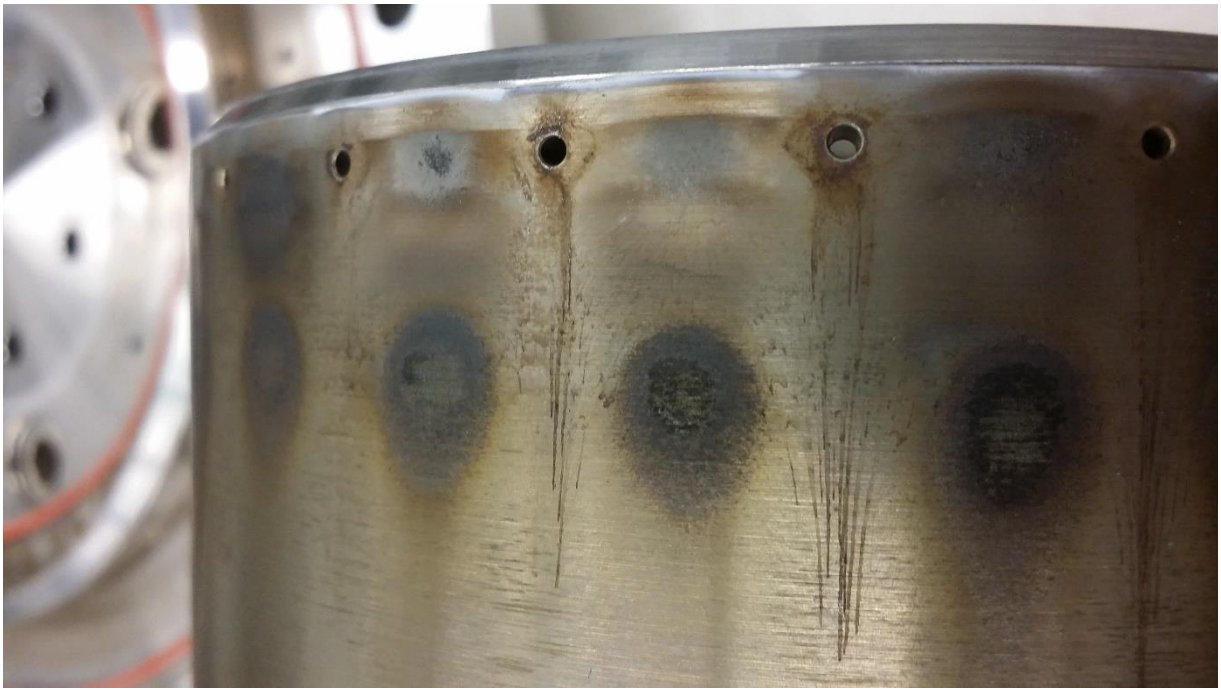

Figure 3.7. Center body outer wall near injection holes after nearly 100 hot fires.

The darkest, largest area of charring occurred just downstream of and on the wall opposing the O_2 injection holes (Figure 3.7). I suspect that, due to the thermal conductivity of the stainless steel body, hot spots developed on the wall of the center body in the well-mixed region just after the injectors which caused deflagration burning of the reactants before they detonated farther downstream. The char marks did not extend more than 5 cm downstream of the injector holes (Figure 3.8).

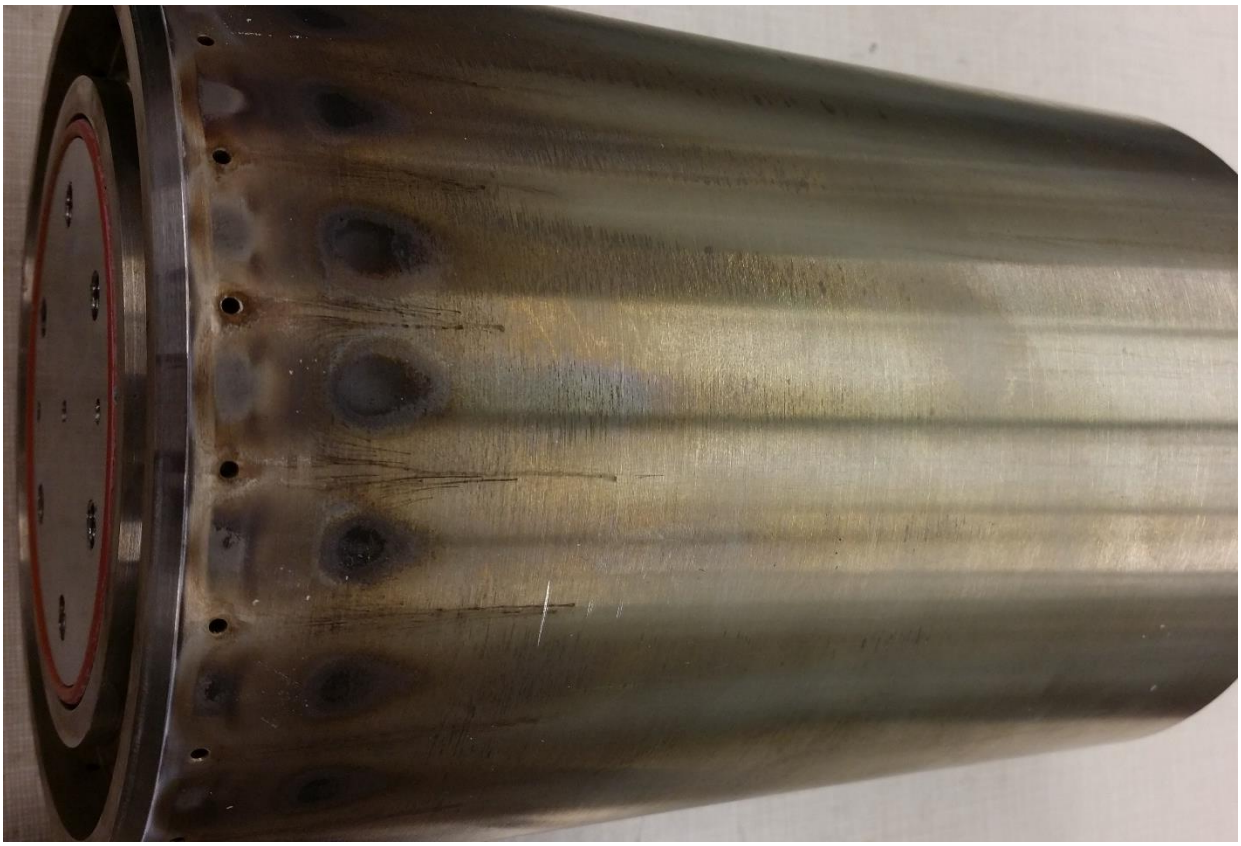

Figure 3.8. Entire center body after nearly 100 hot fires.

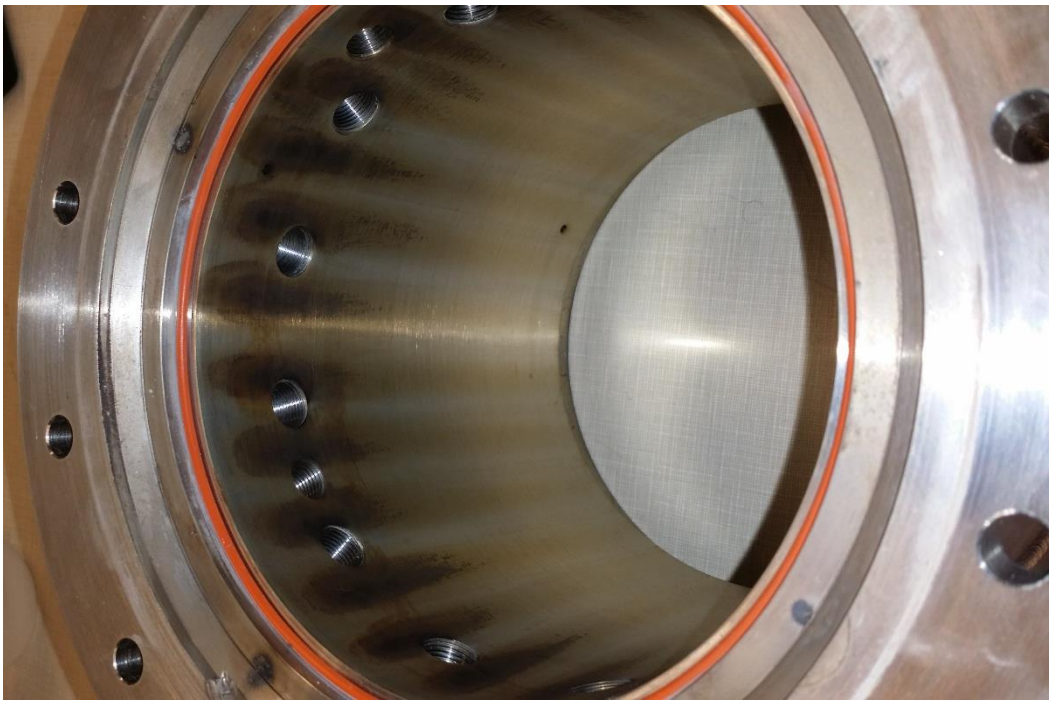

Figure 3.9. Outer body inner wall after nearly 100 hot fires.

The outer body exhibited similar signs of flame-holding (Figure 3.9). The marks on the outer body extended slightly farther downstream than those on the center body. The inner wall of the outer body opposed the H_2 injection holes.

Although pre-burning causes a performance deficit, the more concerning char marks were those found in the manifolds indicating that the manifolds may not have been staying as cool as intended. The manifolds are intended to be isolated from downstream burning by choked orifices. If they were becoming hot enough to burn a potentially reactant mixture inside before passing through the choked orifices, then that posed a safety hazard.

The O_2 manifold exhibited a much greater degree of charring than the H_2 manifold. This is somewhat expected since O_2 is known to oxidize many materials and combust with metals at high temperature, whereas H_2 does not.

Figure 3.10. Interior of the H_2 manifold (end view of the center body) after nearly 100 hot fires.

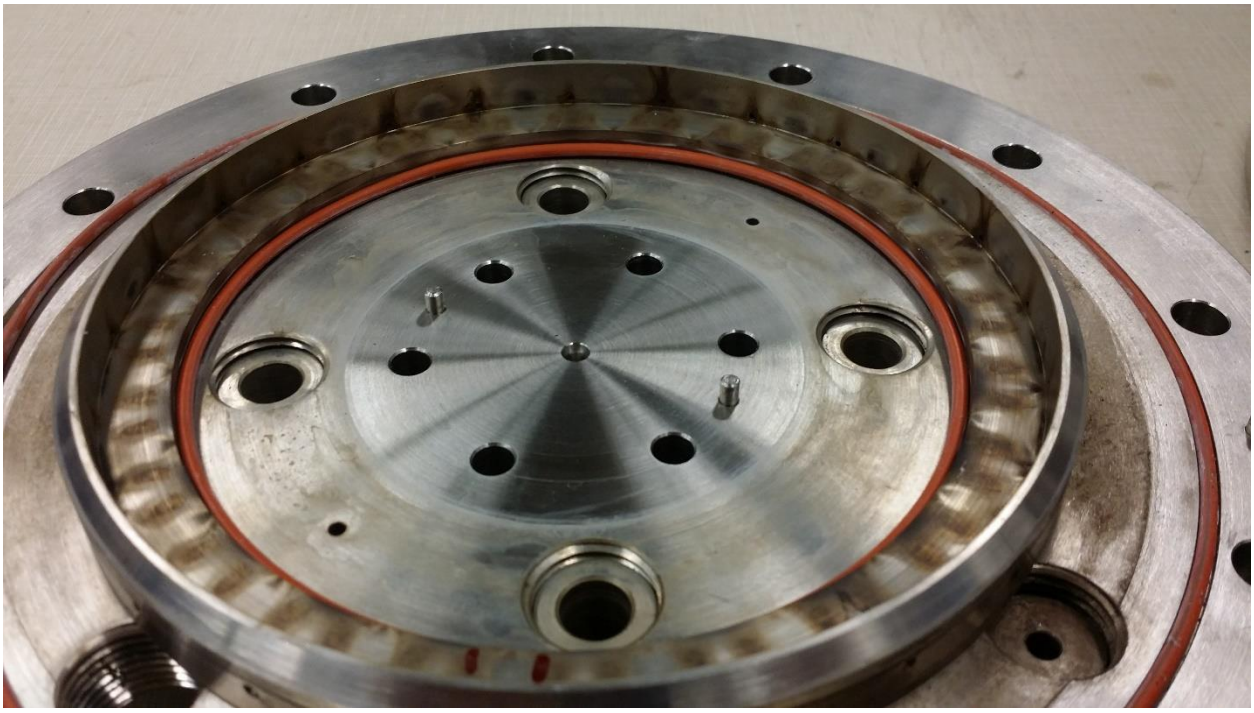

Figure 3.11. Interior of the O_2 manifold after nearly 100 hot fires.

3.7 Spark Plug Durability

The spark plugs maintained sparking and engine-starting integrity after hundreds of runs. Toward the end of testing, I ran in a multiple pulse configuration, allowing very little cooling time and high temperatures for interior parts of the CRDE. The spark plugs had a look similar to Figure 3.12a near the beginning of testing; some discoloration and disintegration of the spark plug surface was visible. After hundreds of runs with some that were mistakenly allowed to spark for much longer than the electronics were designed, the spark plugs took on the very worn look of Figure 3.12b. Tungsten from the electrode coated approximately half of the surface. The other half of the surface exhibits oxidation from the high-temperature, oxygen-rich environment upstream of combustion. Interestingly, the coated surface was always the surface oriented on the downstream side of the spark plug with respect to the wave's spin direction.

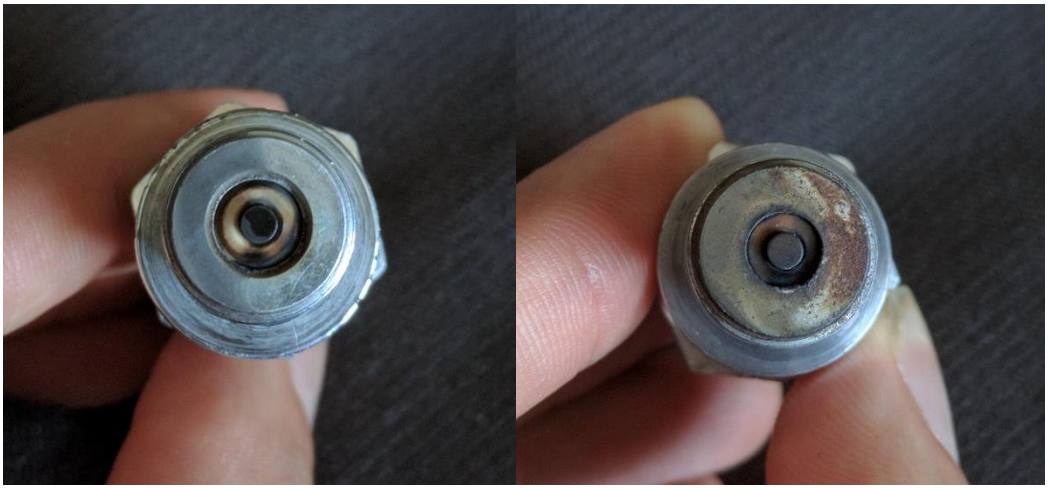

(a) (b)

Figure 3.12. Spark plug surface after approximately (a) 20 s and (b) 100 s of operation.

Chapter 4. ANALYSIS METHODS

The primary diagnostic tools in determining the character of the detonation waves were two high-frequency response PCB® piezoelectric pressure transducers. We used them to sample the pressure in the system at particular locations. After a charge to voltage converter and signal amplifier, LabVIEW directly read the signal through the Data Acquisition (DAQ) interface. A representative signal is provided in Figure 4.1 below.

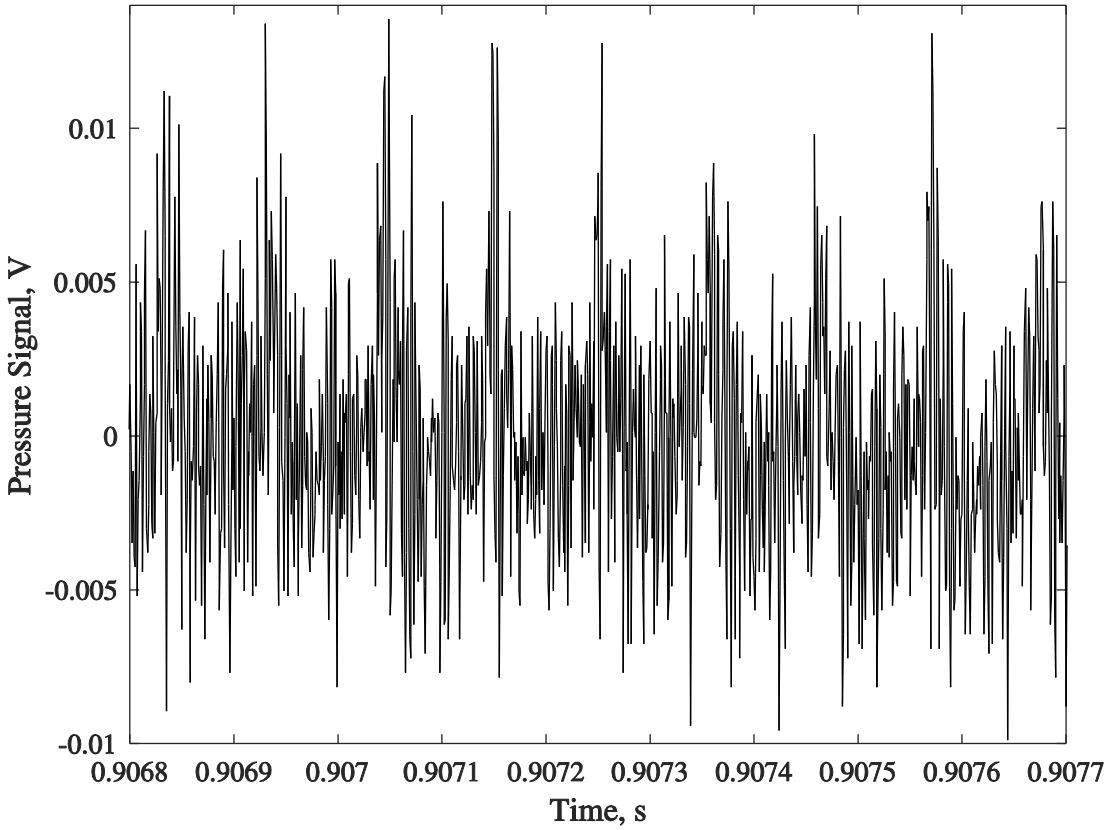

Figure 4.1. Plot of the pressure signal as a function of time for a run in which a 9.5 kHz signal was measured.

The signal was then further analyzed by two distinct techniques: Fast Fourier Transform (FFT) and a peak-finding routine.

4.1 FAST FOURIER TRANSFORM

By Fourier transforming the signal, I was able to view and analyze dominant signal frequencies as shown in the representative plot of Figure 4.2 below. A dominant frequency was interpreted as the passing frequency of a detonation wave. This passing frequency directly informed me of the number and speed of detonation waves. For instance, I commonly observed a frequency of about 4.5 kHz. Interpreted as a wave speed (i.e. multiplied by the annular circumference), this frequency corresponded to approximately 65% of a calculated CJ speed, which is in the range observed by others. Similarly, if I observed a near-multiple of 4.5 kHz as the most predominant frequency in the spectrum, I interpreted the frequency multiple to indicate multiple waves. This is analogous to a turbine spinning with shaft speed ω radians per second. If there are N turbine blades, a stationary transducer in the lab frame measures a frequency of blade passage $f = N\frac{\omega}{2\pi}$, so the rotational frequency of just one blade, i.e. the shaft frequency, is $\frac{f}{N}$. In the CRDE, detonation waves take the place of blades and the shaft is imaginary.

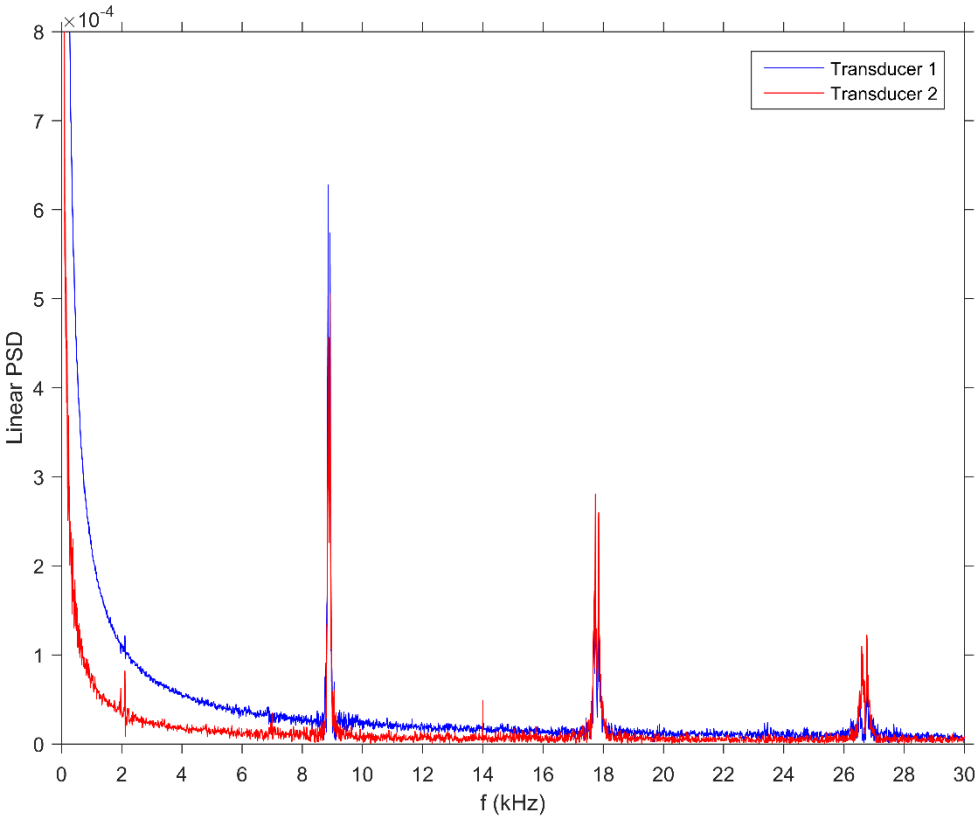

Figure 4.2. Pressure signal as a function of frequency for a run in which an 8.5 kHz signal was measured at location E.

4.2 SPECTROGRAM

A FFT must be calculated over a definite time window, i.e. using a definite number of samples. This limitation means that important indications of long-term stability could be missed because the chosen time window was too short, or short-term phenomena could be missed because the chosen time window was too long and the phenomenon had been averaged away by the transform. To address this shortcoming, while using the same valuable PCB® signal, I used a similar signal processing technique called a spectrogram.

The spectrogram is, at its essence, a series of FFTs which have been calculated over small, overlapping time windows. Viewing FFTs in this way means I could view the frequency response of the sensor as a function of time. Because a FFT provides a two-dimensional plot of Power Spectrum Density (PSD) as a function of frequency, a spectrogram is necessarily a three-dimensional plot of PSD as a function of frequency and time. Most commonly, the frequency and time are represented by the ordinate and abscissa, respectively (though occasionally reversed). The PSD is then represented by a color gradient. As in all plots of PSD, the PSD may be represented on either a logarithmic (dB) or linear scale. I represent the PSD of FFTs using a linear scale and spectrograms using a logarithmic scale. Figure 4.3 below provides a representative spectrogram of the signal from a pressure transducer at location E. Later figures show the spectrograms of both transducer signals.

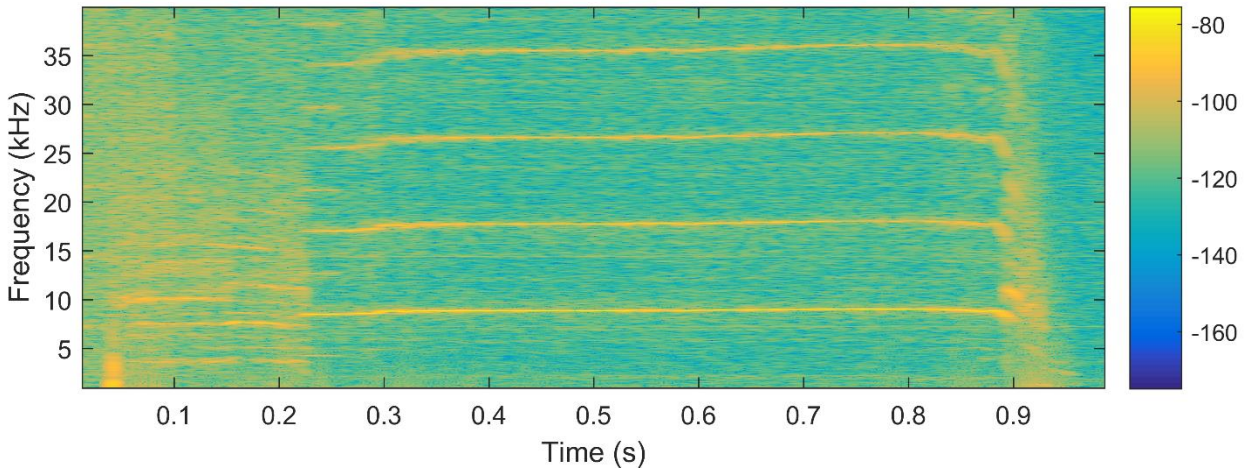

Figure 4.3. Spectrogram of the pressure signal for a run in which a 9 kHz signal was measured. Scale is in dB. The time limits encompass the entire duration of combustion during that run. Note harmonics of the lowest (fundamental) frequency are evident.

4.3 PEAK FINDING (TIME OF FLIGHT)

The second pressure transducer signal analysis method I used was the time of flight measurement technique. The objective of using the time of flight is to detect any spin reversal of the wave during test runs. The method requires two pressure transducers located at the same axial position, but different azimuthal positions. As the wave spins around the engine, it passes one of the transducers at time t and it passes the other transducer at time $t+\Delta t$. The difference between these two times is of course Δt, the "time of flight" of the wave from one transducer to the other. Given a known, fixed distance between the transducers, the wave speed and direction can be determined from the time of flight.

In order to determine the time at which the wave passes a transducer, some procedure must be used to identify the peaks and compare times. Identifying the thousands of peaks per second in the pressure transducer signal is not trivial because the signal data are noisy. MATLAB offers a peak finding routine *findpeaks* which establishes a baseline from which to measure the prominence of adjacent peaks [17]. The user specifies a prominence threshold which must be exceeded in order for *findpeaks* to identify a point as a peak. The user may also specify a minimum number of samples between peaks within one sensor's signal. After finding a peak, the function will not look for new peaks within this minimum number of samples of the last peak. These parameters must be tuned for the signal being analyzed.

After peaks have been found and their times have been recorded, the time of flight may be determined by subtracting the times of peaks from each sensor, $\Delta t_k = t_{2,j} - t_{1,i}$. This must be done element-wise because the peak-finding routine may not have found the same number of peaks in the signal from each transducer, i.e. the peak-finding routine may have missed some peaks. In light of this, if the time of flight is found to be greater than some cutoff value, then that difference is disregarded, t_1 is incremented, and the difference is calculated again. If the time of flight in only one direction is desired, then there could also be a criterion that the time difference be positive. If all criteria are met, the time of flight is recorded, and both t_1 and t_2 are incremented. The next difference is then calculated and so on until the end of one of the peak time records is reached. The MATLAB code for this routine is given in Appendix B. Figure 4.4 provides a representative, nearly ideal plot of the time of flight between two sensors with 240° offset (in the direction of wave

motion). Note that four detonation waves were observed in this run, so the time of flight measured the time from one transducer detecting a wave until the second transducer detected the nearest wave, which was not the same wave that the first transducer detected. This resulted in a shorter time of flight than would be observed in the case of one wave and was a limitation of the spacing of the transducers.

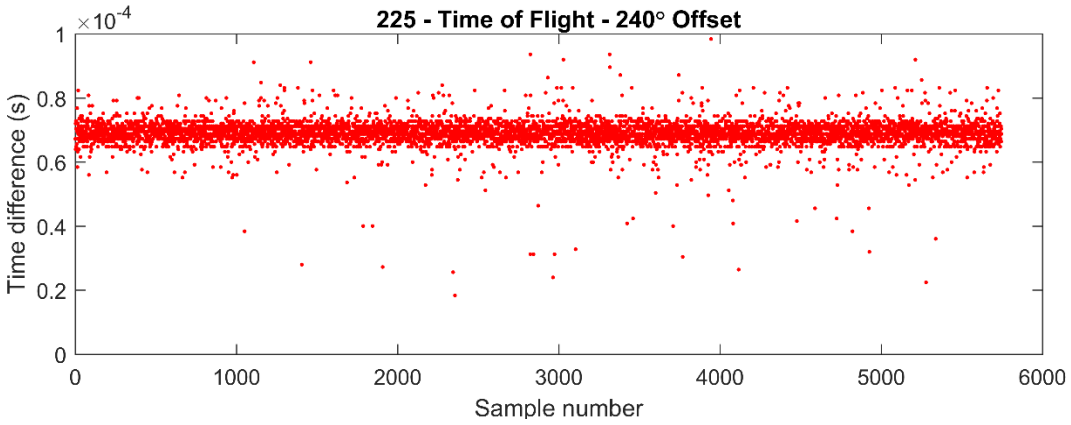

Figure 4.4. Time of flight data for a run with N=4 and sensors offset 240°.

For most runs, the time of flight data were too noisy or inconclusive to reliably determine wave speeds, so time of flight data were only used to determine wave reversal in one test.

Chapter 5. RESULTS AND DISCUSSION

I applied the analysis methods of Chapter 4 to the data from experiments run under many different operating parameters. Some runs did not achieve any steady state, or the frequency data were inconclusive as to a dominant frequency. These runs are included in Appendix C but they are not included in the following presentation of results.

5.1 WAVE SPEEDS

The frequency spectra converted into wave speeds from several representative runs are given in Figure 5.1. The spectra come from a transducer located at E (Figure 3.5). They demonstrate that wave speed decreases at higher wave numbers. This may be attributable to higher (oblique) shock losses and larger areas of deflagration burning which consume the fuel that would otherwise propel the detonation wave.

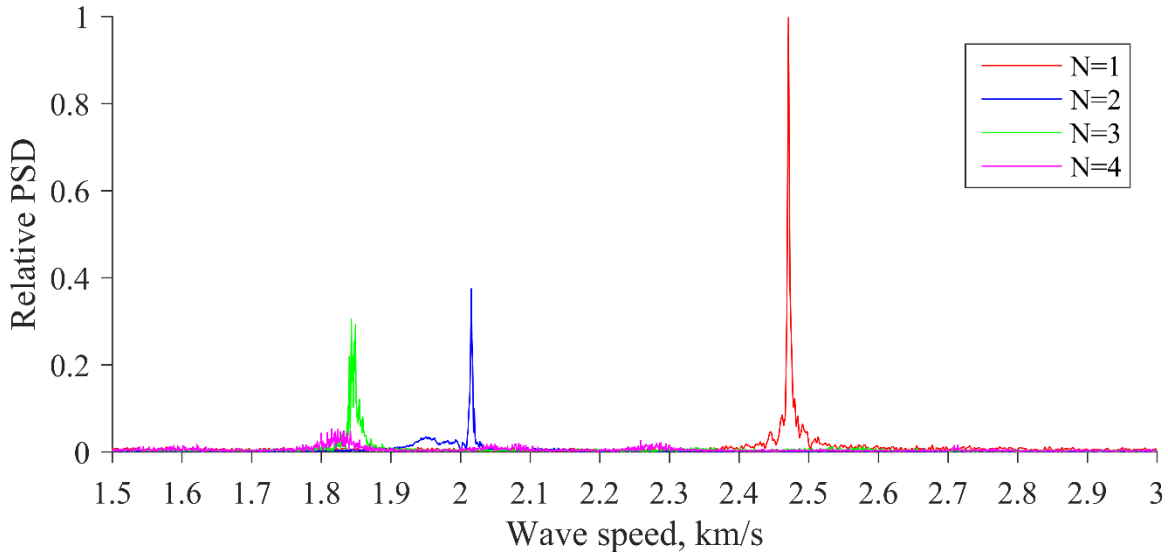

Figure 5.1. Measured wave speeds and relative PSDs for 1-4 detonation waves.

Figure 5.1 also demonstrates that the amplitude of the signal decreases with more waves. This may be in part due to the higher flow rates required for the larger number of waves. It is likely that these flow rates tend to push the detonation farther downstream in the engine away from the pressure transducers perhaps by delaying mixing in the axial direction. This issue will be examined further in future testing.

Finally, this figure demonstrates a means to investigate the phenomenon of wave reversal that Russo observed [18]. Wave reversal would manifest as a secondary frequency lower than the dominant frequency (the wave takes longer than usual to travel past the transducer), but this is not observed. This may be attributable to the lack of an opening for the pre-detonator tube in the UW CRDE which could interact with the detonation waves.

5.2 Simultaneous Spark Influence

The results of the tests correlating N_{dr}, the number of driving simultaneous sparks or "spark waves," with the observed predominant frequency of detonation waves are presented in Figure 5.2. Each point corresponds to one test run where one prominent wave frequency was observed. The results demonstrate that the wave generator has very little impact on the number of detonation waves generated; any of the three tested simultaneous spark settings could generate virtually any frequency (wave speed or number of waves). Instead, it appears that the wave generator plays the primary role of a starter for the engine.

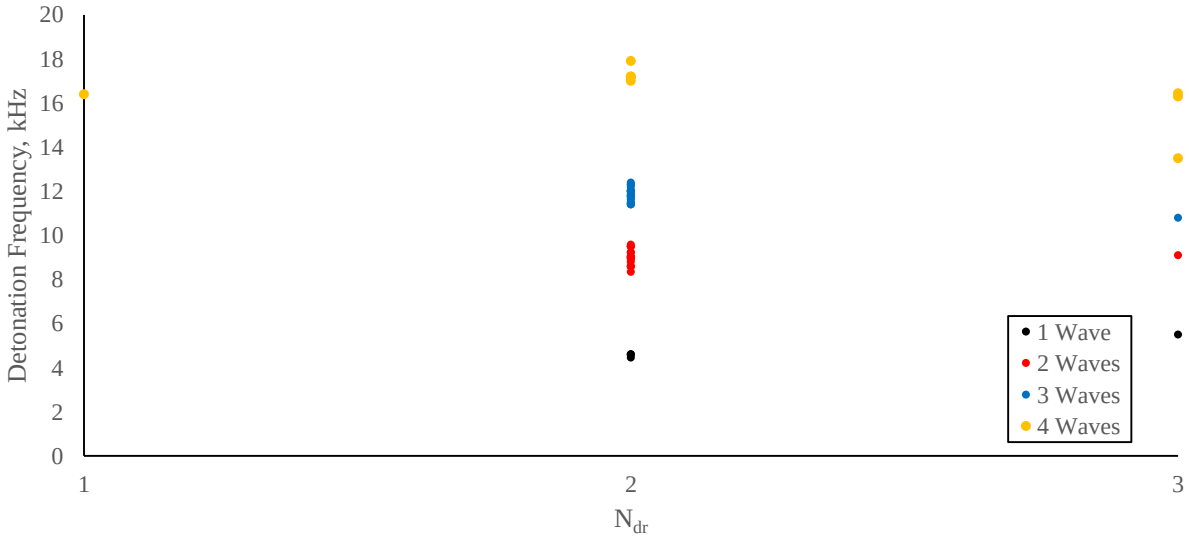

Figure 5.2. Plot of detonation spin frequency as a function of number of simultaneous sparks.

5.3 Flow Rate

The number of detonation waves exhibited strong dependence on flow rate. A plot of this relationship is provided in Figure 5.3. As in Figure 5.2, each point corresponds to one test run where one prominent wave frequency was observed. A clear correlation exists between increasing flow rate and increased number of waves.

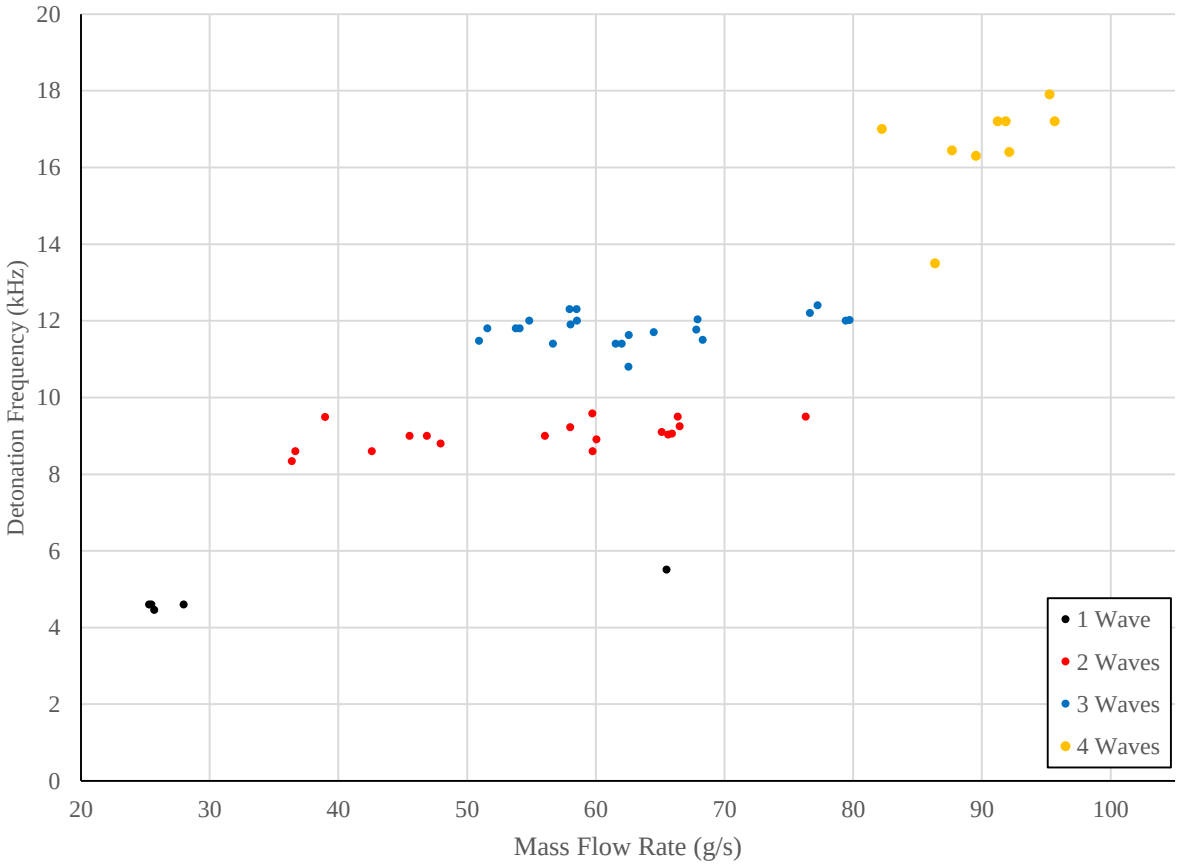

Figure 5.3. Detonation frequency plotted as a function of mass flow rate. As expected, increasing mass flow could support higher numbers of detonation waves.

5.4 Equivalence Ratio and Wave Speed

Chapman-Jouguet detonation wave speeds depend on equivalence ratio. In H_2 and O_2 mixtures, an increase in the mass fraction of H_2 will increase the mixture's sound speed and thereby increase detonation wave speed. Because of this, I expected to observe a similar dependence on equivalence ratio for this experiment. The plot of D_{spin} vs. equivalence ratio in Figure 5.4 demonstrates this same dependence in the experiments I conducted. The data exhibit a weak positive correlation.

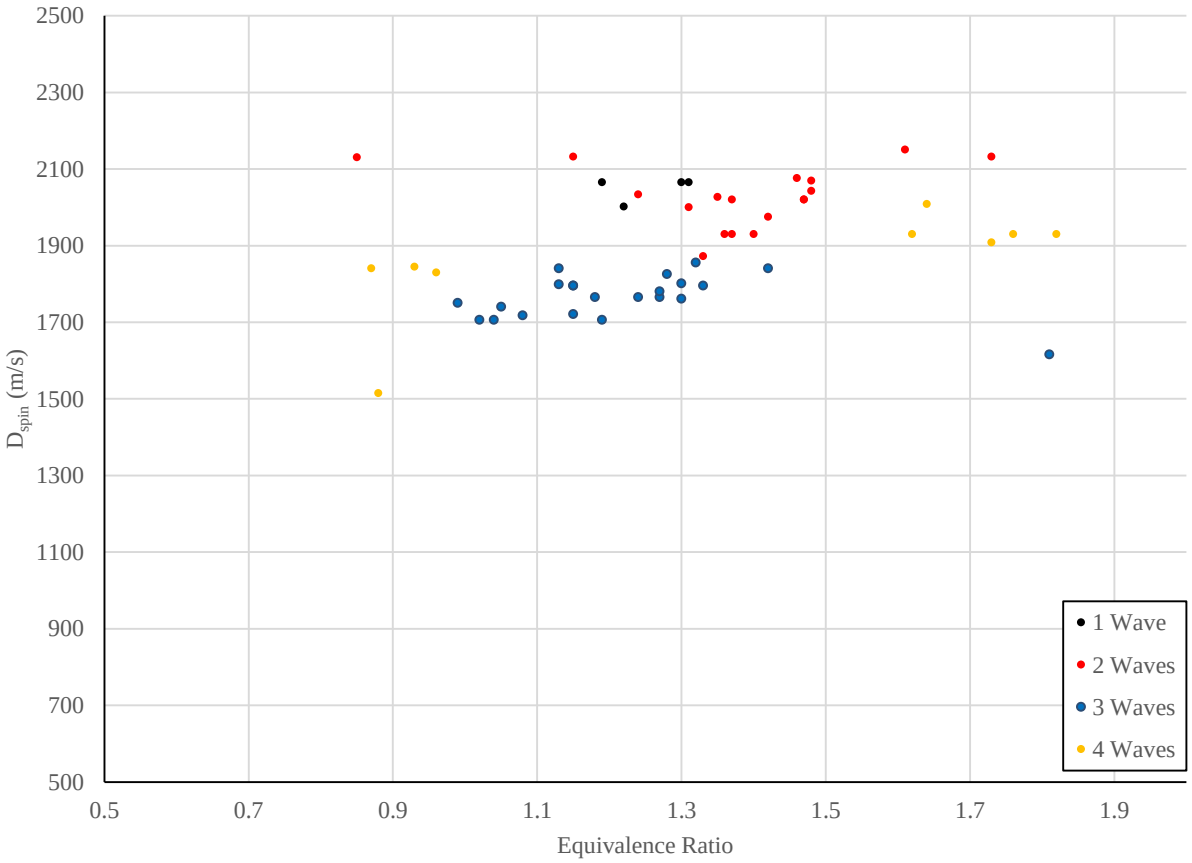

Figure 5.4. Detonation wave speed as a function of equivalence ratio.

If the wave speed is considered as a proportion of CJ velocity, the data show almost no correlation between equivalence ratio and D_{spin}/D_{CJ} as in Figure 5.5.

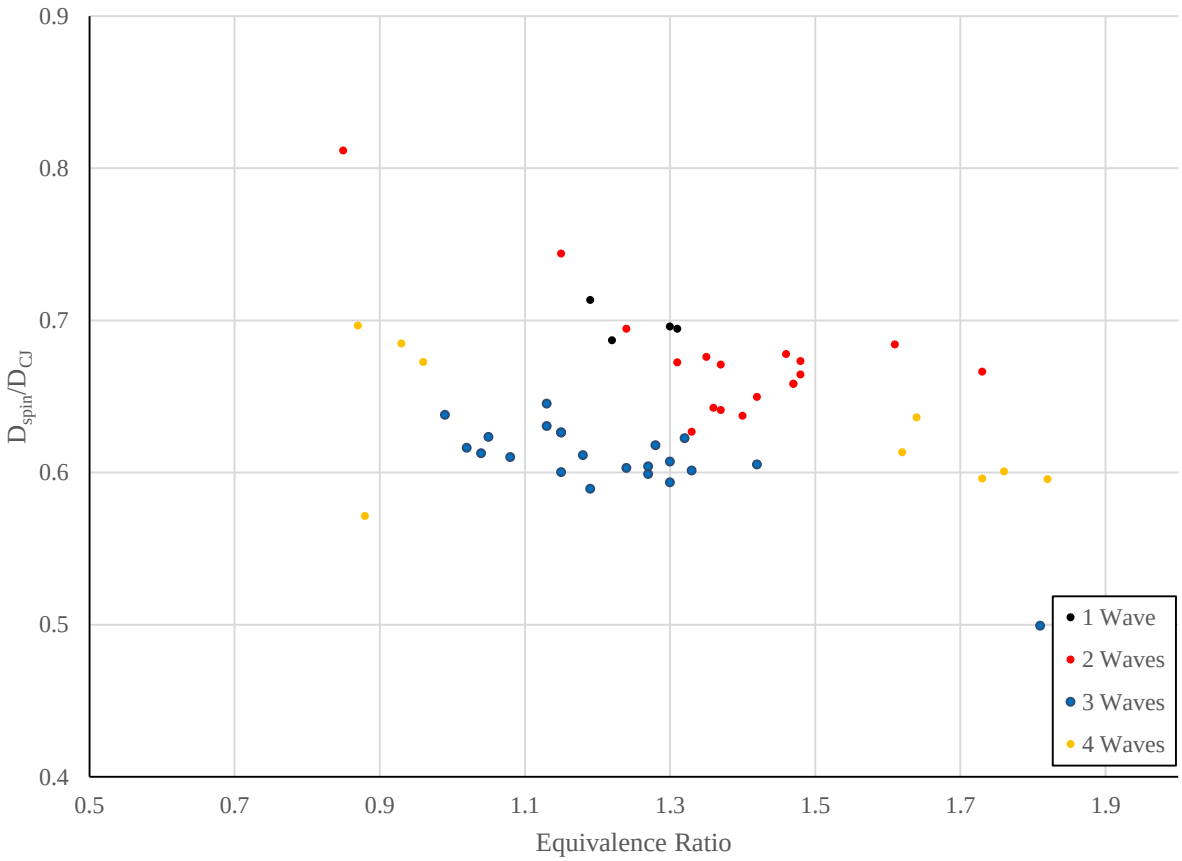

Figure 5.5. Detonation spin speed normalized by Chapman-Jouguet velocity as a function of equivalence ratio.

5.5 Number of Waves

The normalized detonation spin speed was compared with the number of detonation waves and demonstrates a tendency to decrease with increasing number of detonation waves. This might indicate that areas of deflagration pre-burning are relatively larger when flow rates and number of detonation waves are higher.

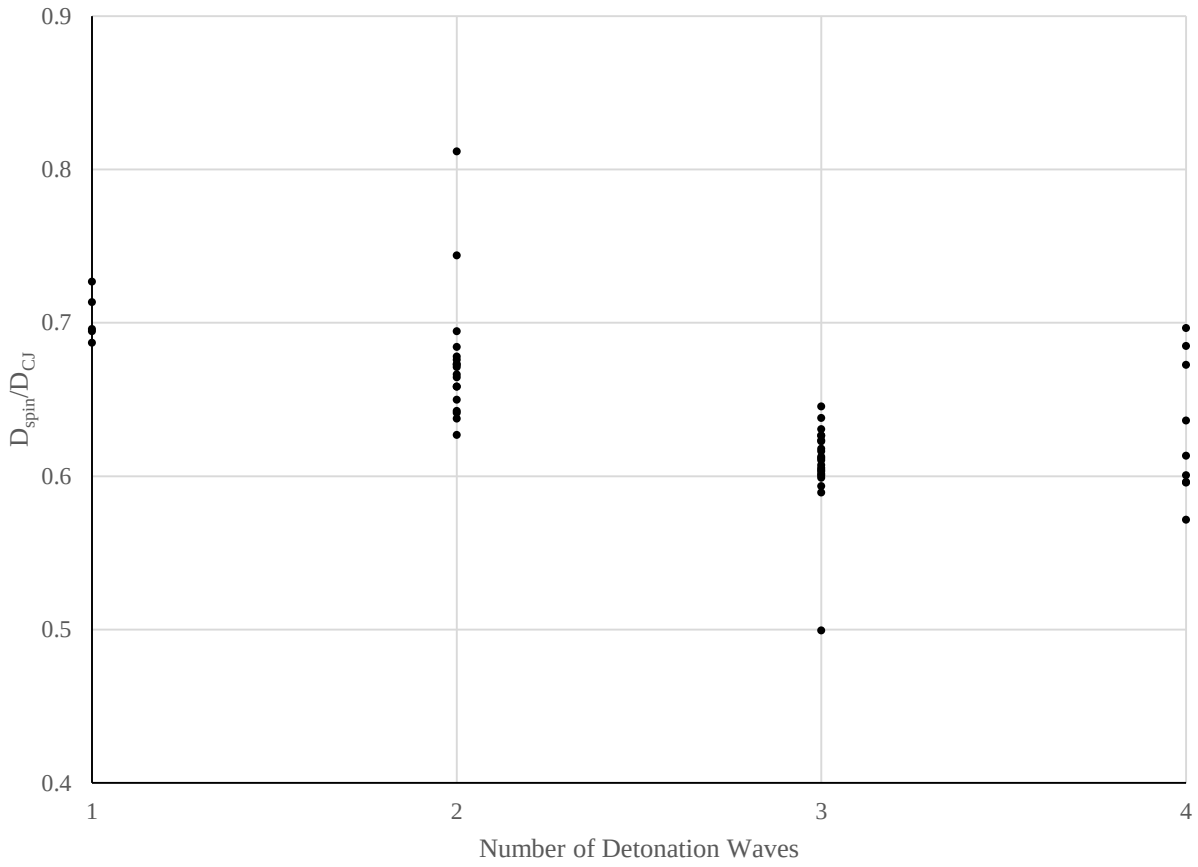

Figure 5.6. Detonation spin speed normalized by Chapman-Jouguet velocity as a function of number of detonation waves.

5.6 SPARKING DIRECTION

The wave generator had the capacity to reverse the order of sparking so that sparks could either fire in a clockwise or counterclockwise sequence as viewed from the head end of the CRDE as in Figure 3.5. In order to establish the efficacy of the wave generator in driving a detonation wave in a particular direction, transducers were located at positions A and E in Figure 3.5. I then performed two tests: one in which the sparking sequence was counterclockwise (Figure 5.7), the other in which the sequence was clockwise (Figure 5.8). I calculated the time of flight by subtracting the arrival time of transducer E from transducer A, so positive times corresponded to counterclockwise direction of detonation wave travel. By examining the sign of the time of flight between the two piezoelectric transducers, I determined the direction of travel of the wave. The test results demonstrate that the direction of sparking corresponded to the direction of wave travel.

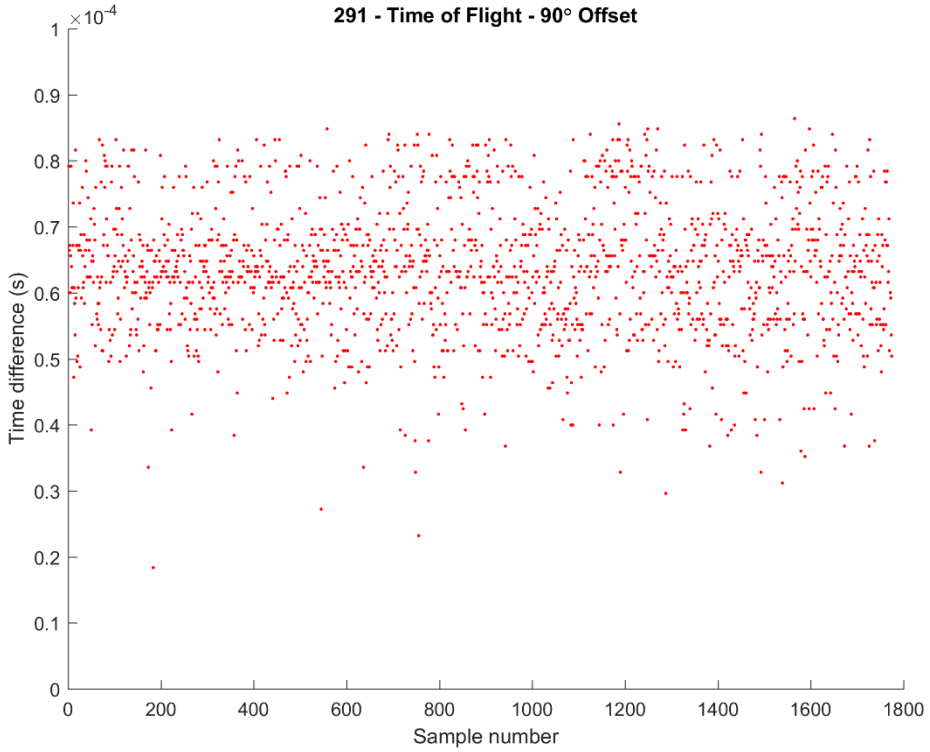

Figure 5.7. Time of flight for N=1 after counterclockwise sparking.

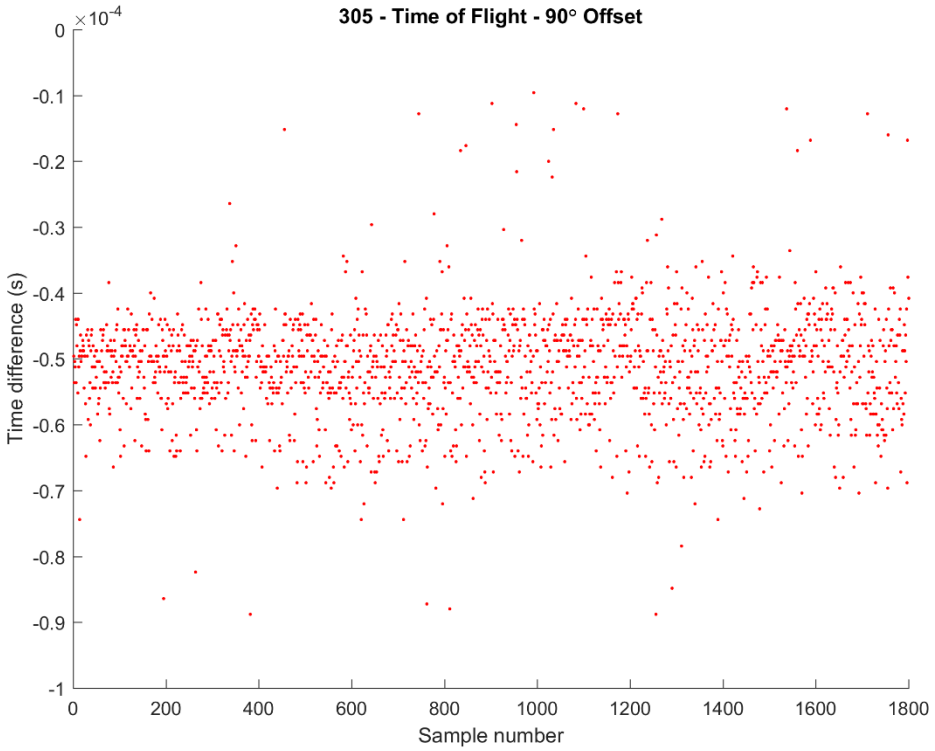

Figure 5.8. Time of flight for N=1 after clockwise sparking.

5.7 SPARSE SPARKING

In determining the minimum number of sparks which could create a stable detonation wave, I ran the experiment in three different sparking configurations. Considering the spark plugs to be numbered sequentially around the azimuth from 1 to 12, the first test was to run with active sparks plugs only in positions 1, 3, and 5. Figure 5.9 shows the result of this test. Transducers were located at locations E (top spectrogram) and A (bottom spectrogram).

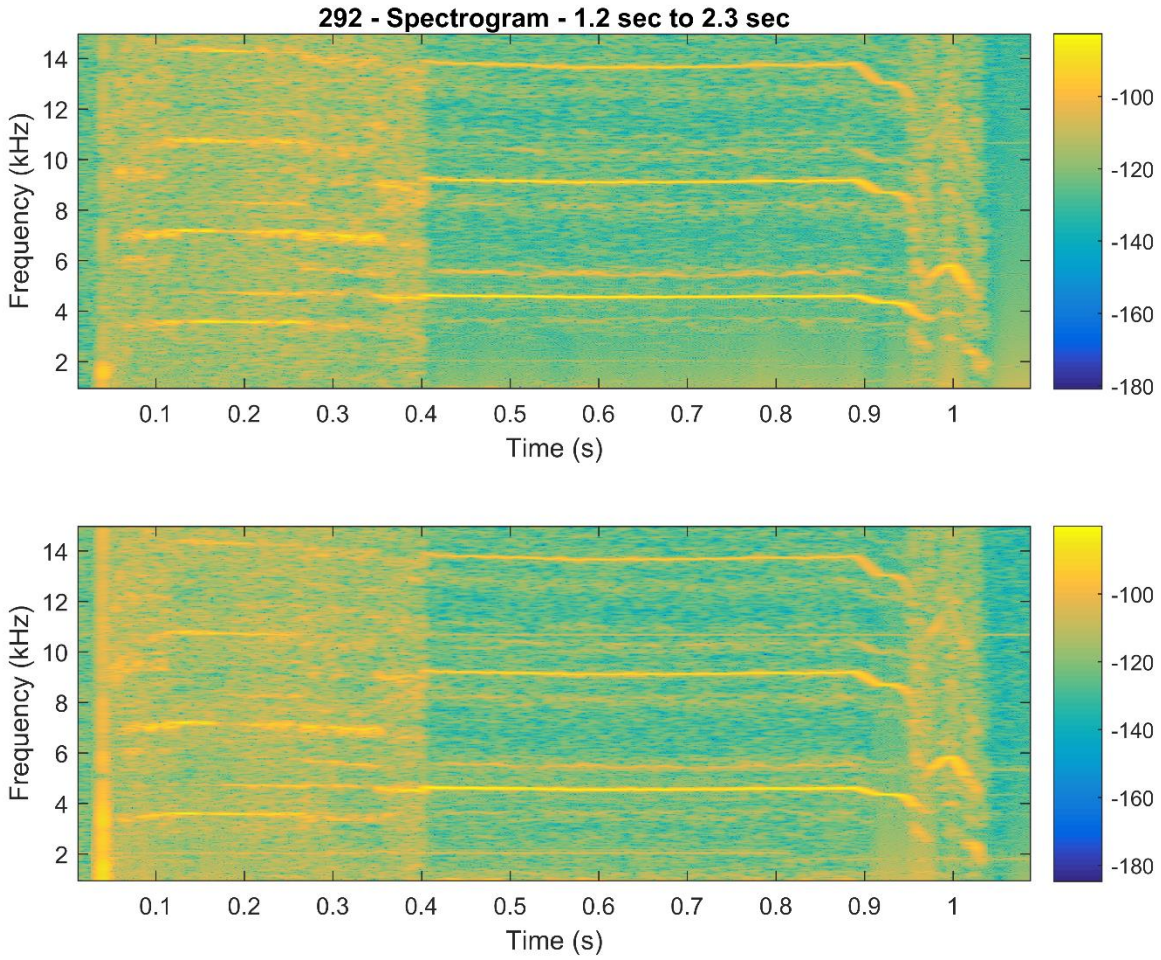

Figure 5.9. Spectrogram of a run which was ignited by three sparks located at positions 1, 3, 5.

Some deviation from constant wave speed is evident by the appearance of sidebands. A nearly 5 kHz signal corresponding to N=1 is observable.

The second sparking configuration had three active spark plugs equally spaced around the CRDE in positions 1, 5, and 9. The results of the test of that configuration are given in Figure 5.10. The

results indicate that the CRDE never achieved a highly stable operating mode, the fundamental frequency 3.6 kHz is slower than the usual N=1 case, and sidebands are very prevalent indicating offset in the wave positions from uniform spacing. This result indicates that some stability was lost due to spark spacing becoming too large.

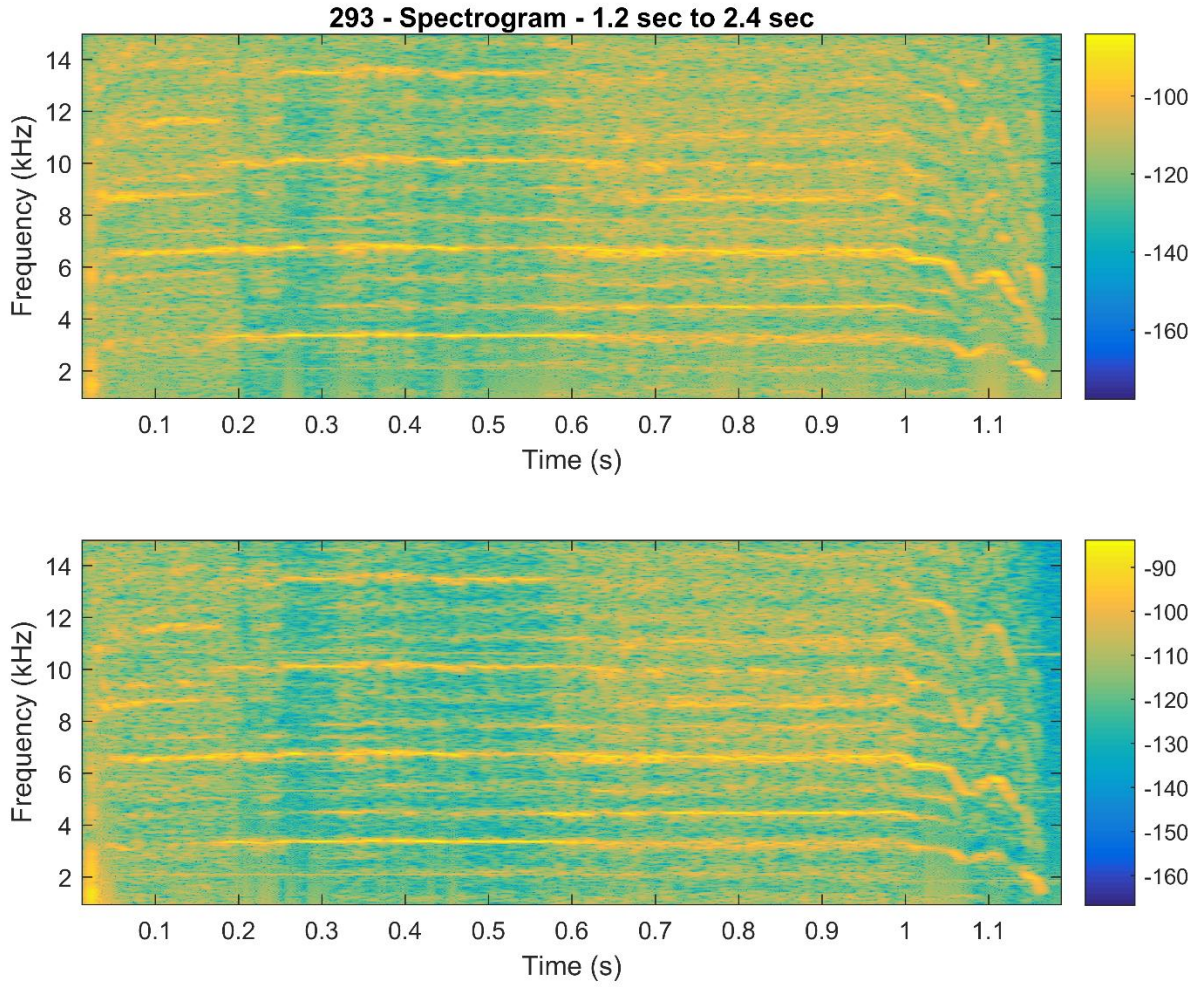

Figure 5.10. Spectrogram of a run which was ignited by three sparks located at positions 1, 5, 9.

The third and final sparking configuration was to use only spark plug in position 1. The resulting spectrogram from the experiment conducted in this configuration is given in Figure 5.11. The result was somewhat similar to the result shown in Figure 5.10 in that a single sideband indicates the wave may have been changing direction frequently. Like Run 293, the fundamental frequency is lower than the usual 4.5 kHz observed for N=1. This, in combination with the other frequency bands, may indicate frequent wave reversal or counter-rotating waves.

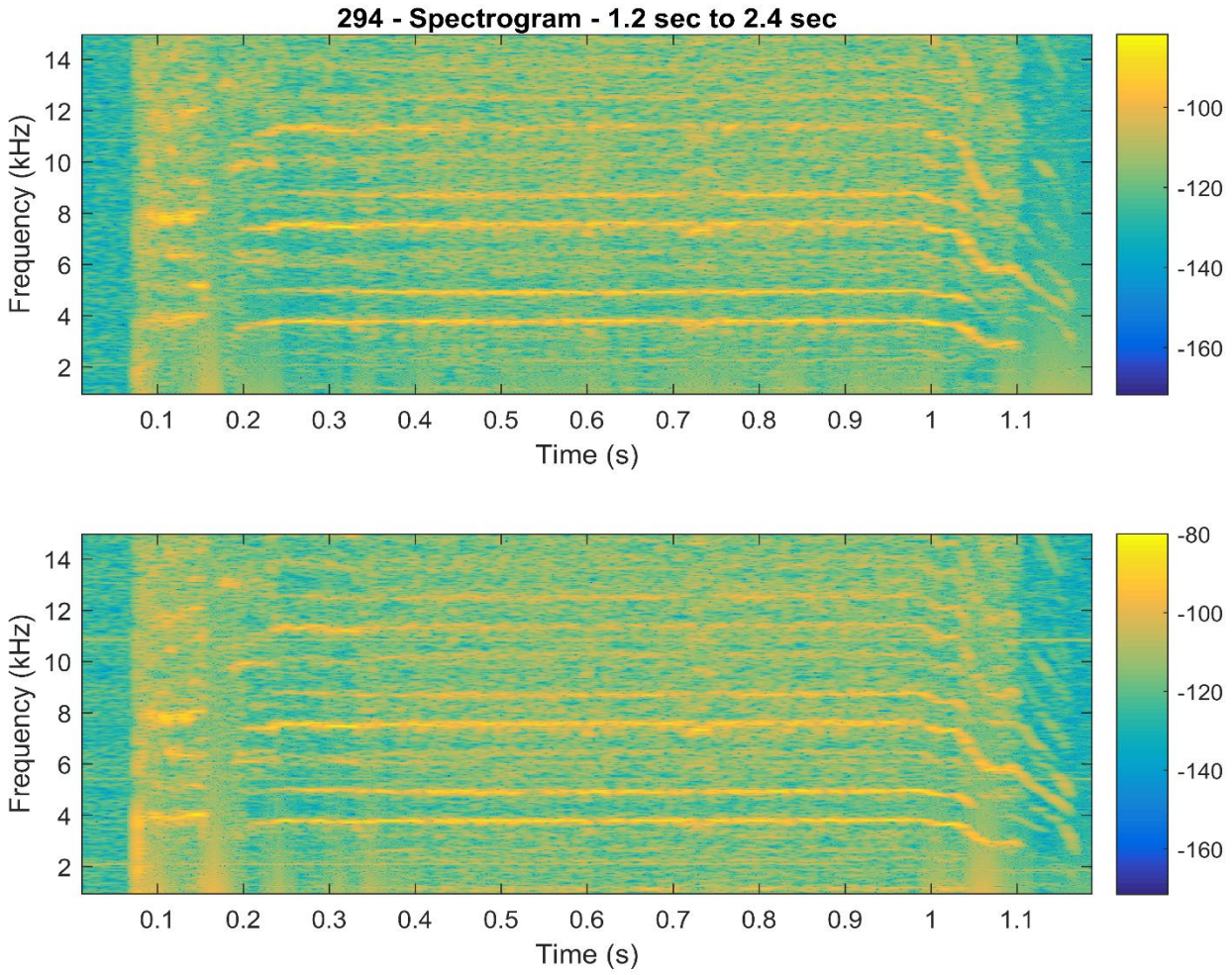

Figure 5.11. Spectrogram of a run which was ignited by only one spark.

Chapter 6. CONCLUSION

6.1 Summary and Concluding Remarks

The sparking and mixing methods devised for the CRDE have been successfully demonstrated. Sequential sparking in the azimuthal direction, at a rate near the sound speed of a gaseous H2/O2 mixture, was successful in initiating spinning detonation waves. These detonation waves did not interfere with the reactant injection process because of a novel radial-injection mixing scheme which delayed mixing in the axial direction downstream of the sparking device. The total flow rate was shown to have a strong influence on how many detonation waves were observed. The number of simultaneous sparks did not demonstrate any influence on the number of observed detonation waves. The exact position of the detonation waves in the CRDE and the observed pressure signal strength were influenced by the total flow rate; i.e., as the detonation waves moved axially downstream with increasing flow rate, their signal strength decreased.

6.2 Recommendations for Future Research

In future work with the UW CRDE, the following areas have been identified which may be researched.

6.2.1 *Locate axial location and length of detonation zone*

The results of my research indicate that the length of the detonation zone increased in order to combust all of the reactants while the detonation wave number and speed remained constant over a range of flow rates. Future research could focus on determining the relationships which cause the detonation zone to lengthen and move axially within the combustor.

6.2.2 *Measure thrust-producing pressure over front combustor wall*

The bulk of the thrust in the CRDE will be generated by oblique shock waves which propagate toward the front wall of the combustion chamber. The pressure of these waves will act to provide thrust for the CRDE. Future research may determine the relationship of this thrust-producing pressure to other variables such as those I have presented in Chapter 5.

6.2.3 *Test wave generator with JP fuel and air*

For ultimate application and acceptance as a propulsion engine, the CRDE must be able to use the ubiquitous fuel and oxidizer combination of JP fuel and air. Future testing on the UW CRDE should establish whether the wave generator can detonate this atomized liquid fuel in such a dilute oxidizer.

BIBLIOGRAPHY

[1] Meholic, G., “Potential Applications of RDE Technology in Liquid Rocket Engines,” *presented at* The UCLA-Purdue Technical Interchange Meeting on Rotating Detonation Engine (RDE) Technology, UCLA, June 18, 2014.

[2] Stechmann, D., Kan, B. N., Lim, D., and Heister, S., “Rocket Applications of PGC: An Introduction,” AIAA Propulsion and Energy 2015,Orlando, FL 27-29 July, 2015.

[3] Vidal, P. “Basics of detonation dynamics in gases: phenomenology, models and propulsion,” GEA Summer Program, Poitiers, France, 25 June, 2014.

[4] Heiser, W.H. and Pratt, D.T., "Thermodynamic Cycle Analysis of Pulse Detonation Engines", Journal of Propulsion and Power, Vol. 18, No. 1 (2002), pp. 68-76.

[5] Smith, R.D., “Experimental Investigation of CDREs for In-Space Propulsion,” GHKN Engineering, LLC, AIAA Propulsion and Energy 2015, Orlando, FL 27-29 July, 2015.

[6] Canteins, G., “Etude de la détonation continue rotative - Application à la propulsion,” Energie électrique. Université de Poitiers, 2006. Français.

[7] Claflin, S., Stout, J., Lynch, E. D., “Rotating Detonation Engine Development for Rocket Applications at Aerojet Rocketdyne,” AIAA Propulsion and Energy Forum, Orlando, FL, 27-29 July, 2015.

[8] Kasahara, J., “500-N Class Rotating Detonation Rocket Engine Experiment and Sounding Rocket Flight Program,” AIAA Propulsion and Energy Forum, Orlando, FL, 27-29 July, 2015.

[9] Cho, K. Y., Codoni, J. R., Rankin, B. A., Hoke, J. L., Schauer, F.R., “High-Repetition-Rate Chemiluminescence Imaging of a Rotating Detonation Engine,” AIAA 2016-1648.

[10] Wilhite, J., Driscoll, R., St. George, A., Anand, V., Gutmark, E. J., “Investigation of a Rotating Detonation Engine using Ethylene-Air Mixtures,” AIAA 2016-1650.

[11] Anand, V., St. George, A., Gutmark, E. J., “Hollow Rotating Detonation Combustor,” AIAA 2016-0124.

[12] Stoddard, W. A., St. George, A., Driscoll, R., Anand, V., Gutmark, E. J., “Experimental Validation of Expanded Centerbodiless RDE Design” AIAA 2016-0128.

[13] Andrus, I. Q., King, P. I., Polanka, M. D., Schauer, F. R., Hoke, J. L., “Design of a Premixed Fuel-Oxidizer System to Prevent Flashback in a Rotating Detonation Engine,” AIAA 2016-0127.

[14] St. George, A., Driscoll, R., Anand, V., Gutmark, E.J., AIAA "Starting Transients and Detonation Onset Behavior in a Rotating Detonation Combustor," AIAA 2016-0126.

[15] Pandiya, N., St. George, A., Driscoll, R., Anand, V., Malla, B., Gutmark, E. J., "Efficacy of Acoustics in Determining the Operating Mode of a Rotating Detonation Engine," AIAA 2016-1649.

[16] Heath, J. D., "Generating Detonation Waves in an Annulus via Phased Adiabatic Shocks," University of Washington, Seattle, Washington, 2015.

[17] MATLAB and Signal Processing Toolbox Release 2015b, The MathWorks, Inc., Natick, Massachusetts, United States.

[18] Russo, R. M., "Operating Characteristics of a Rotating Detonation Engine Using Hydrogen and Air," Air Force Institute of Technology, Wright-Patterson Air Force Base, Ohio, 2011.

APPENDIX A: PRE-RUN CHECK LIST

Pre-Run Check List: Date: _____ Run #: _____ Initials: _____

Physical Checks:

- Shop air turned "on", valve above the air hose should be in the upwards facing position
- Gas cylinders connected: N_2 6-pk, O_2, H_2
- Before KT-300 vacuum pump operation
  - Check oil level: 3/8" above bottom of sight glass
  - Close final dump tank water drain valves (bottom) and both vent valves (top)
  - With pump isolation valve closed, turn on pump, check oil again, open isolation valve
  - If open, close water drain valves in exhaust lines
  - Record Butterfly Valve setting: _____
  - Were there any instrumentation problems in the last run? Replace if necessary.

Pre-Run VI Actions:

- Close all unnecessary programs besides the LabView VI
- Validate run control sequence with valve control box set to: **DIG DISABLE**
- Validate all sensors are functional (if not fixable, note in instrument log – "Line Names File.xlsx")
- Validate ram lab CRDE VI is running and **armed** (via RDP) and seeing correct pressure transducers
- Check that data files from prior run are removed from "Data Files" folder
- Make new run folder (XXX) and backup folder (20xx-xx-xx-run#)
- Update the run comments file with any instrumentation changes or notes

Pre-Run Physical Actions:

- Confirm nominal operation of H2/O2 flow control in prior run; if not,
  - Readjust regulators if flow ratio is off
  - Cycle H_2* and O_2 valves (switch 15 & 16) if valve hang up detected

    *** Make sure the H_2 line is vented upstream before cycling valve #15!**
- Power cycle the signal transfer box (if the DAS is not reading correct values)
- Set up camera(s) (if being used)
- Check vacuum is complete (< 9 kPa in reactor)
- Turn water on to PCB's

Final Actions Before the run:

- Verify wave number is selected to the correct value (N=1,2,3, or 4), N = _____
- Verify wave controller power supply is on at 167 volts
- Shut off the KT-300 vacuum pump (close valve before shutting off pump)
- Start camera(s) (if being used)
- Validate spark freq generator system is controlled by VI at desired Hz, frequency = _____ Hz

Pre & Post Run Data to Record

Record:	**Initial**	**Final**	**Cylinders Used**
o N_2 Cylinder(s) pressure:	_____ psig	_____ psig	Row ____ Cyl's ____
o O_2 Cylinders pressure:	_____ **kPa**	_____ **kPa**	
o H_2 Cylinders pressure:	_____ **kPa**	_____ **kPa**	
o N_2 (B) Cylinder(s) pressure:	_____ psig	_____ psig	

- Close both doors to the shockwave reactor lab (201/239)
- **Set switch on solenoid controller box to: DIG ENABLE**
- *Safety Glasses!*

NOTE: in case of no-ignition, manually fill system to 70-100 kPa with N2 by opening switch 4 and monitoring VT gauges

Post-Run Check List:

Immediately after the run:

- Turn off digital disable switch on Solenoid Controller box **after** all automatic valve actions have stopped (~20 sec)

Over the next several minutes:

If no detonation

- Purge system by back filling with N_2 up to at least 50 kPa (use valve 4 if minimum system pressure not reached in experiment)
- Open room vent ball valve above the KT-300 pump ***SLOWLY*** to allow the SWR to fill with air from the room

If detonation

- Open room vent ball valve above the KT-300 pump ***SLOWLY*** to allow the SWR to fill with air from the room

In all cases

- Use KT-300 pump to evacuate purge gas to: < 26 in-Hg or 15 kPa
- After purge evacuation, open Drain Valves at Front and Rear of Dump Tank
- Note final pressure in N_2 6-pk manifold.
- **Close all N_2 cylinders on 6-pk and its manifold isolation valve**
- Open water drain valves on KT-300 exhaust lines
- Shut off PCB water

Check that pressure in the dump tank is atmospheric BEFORE continuing!

- **Vent Hydrogen Manifold to the roof after closing H_2 cylinders**
- **Vent Oxygen Manifold to the room**
- Place the data files into the correct sub-folder after the run has completed (< 1 min)
- Run matlab program to process data

On as needed basis

- Drain water from KT-300 crankcase (may be hot!)
- Separate water from vacuum oil using oil circulation pump (pump 5 minutes, drain – repeat if necessary)

APPENDIX B: TIME OF FLIGHT CODE

```
function []=timeofflight(runnum,time1,time2)
%%%%%%%%%%%%%%%%%%%%%%%%%%%%%%%%%%%%%%%%%%%%%%%%%%%%%%%%%%%%%%%%%%%%%%%%%%%%
% timeofflight
% This code takes in a run number and time interval to determine times of
% flight for the high speed data from both pressure transducers. It returns
% nothing. It prints an average time of flight whose averaging interval
% should be adjusted for each particular run.
%%%%%%%%%%%%%%%%%%%%%%%%%%%%%%%%%%%%%%%%%%%%%%%%%%%%%%%%%%%%%%%%%%%%%%%%%%%%
cwdhost;
fs = 1.25e6; % DAQ sampling rate
detfreq = 5e3; % estimated wave frequency to set max/min period
period = 1/detfreq/4;
idx1 = time1 * fs;
idx2 = time2 * fs;
runstr = num2str(runnum);
t1str = num2str(time1);
t2str = num2str(time2);

plotvar = readcrdedata(runnum,'y');
pcb1 = plotvar.PCB_volt1(idx1:idx2);
pcb2 = plotvar.PCB_volt2(idx1:idx2);

thresh1 = .003; % prominence thresholds for findpeaks()
thresh2 = .004;

[~,t1] = findpeaks(pcb1,'MinPeakProminence',thresh1,'MinPeakDistance',70);
[~,t2] = findpeaks(pcb2,'MinPeakProminence',thresh2,'MinPeakDistance',70);

t1 = t1/fs;
t2 = t2/fs;

deltat = zeros(1,1);
ii = 1;
jj = 1;
kk = 1;

% Loop to examine all elements, subtracting t1 from t2. If t2 is within
% "period" of t1, then that time difference is acceptable. If the time
% difference is less than zero, then that is not an acceptable time
% difference. The index is incremented, and the next element is examined.
% t1 and t2 can be reversed to provide shortest time of flight.
while (ii <= length(t1)) && (jj <= length(t2))
    temp = t2(jj) - t1(ii);

    if temp > 2.5 * period
        ii = ii + 1;
    elseif temp < .1 * period
        jj = jj + 1;
    else
        deltat(kk) = temp;
```

```
        ii = ii + 1;
        jj = jj + 1;
        kk = kk + 1;
    end
end

avgdiameter = 5.62 * .0254;
circumference = avgdiameter * pi();
distance = circumference / 4; % This distance is based on PCB position.
wavespeed = distance ./ deltat;

plottitle = [runstr,' - Time of Flight - ',t1str,' sec to ',t2str,' sec'];
figure;
% Uncomment following lines to make a subplot with wavespeed.
% subplot(2,1,1)
% plot(wavespeed,'.b')
% title([num2str(runstr),' - Wavespeed from Time of Flight - 90\circ
Offset']);
% ylim([1000 3000])
% xlabel('Sample number')
% ylabel('Wavespeed (m/s)')
% subplot(2,1,2)
plot(deltat,'.r')
title([num2str(runstr),' - Time of Flight - 90\circ Offset']);
ylim([0 1e-4])
xlabel('Sample number')
ylabel('Time difference (s)')
set(gcf,'name',plottitle,'numbertitle','off')
print(['..\Time of Flight\',plottitle,'.png'],'-dpng','-r600');

fprintf('Run %i - mean time = %.3e s\n',runnum,mean(deltat(3500:3600)));
end
```

APPENDIX C: RAW DATA OF DETONATED RUNS

run	Ndr	mdot	phi	fdet	Ndet	speed
22	2	66.52	1.46	9.25	2	2075.955
24	2	65.91	1.24	9.06	2	2033.313
25	2	59.73	1.61	9.58	2	2150.016
32	2	56.06	1.37	9	2	2019.848
33	2	60.06	1.31	8.91	2	1999.649
38	2	59.75	1.36	8.6	2	1930.077
40	2	58.01	1.48	9.22	2	2069.222
43	2	67.55	1.31	10.88	3	1627.848
45	2	67.8	1.3	11.77	3	1761.008
46	2	67.9	1.3	12.04	3	1801.405
48	2	65.63	1.35	9.03	2	2026.581
49	3	99.9	1.3	11.7	6	875.2673
50	3	96.36	1.21	11.7	3	1750.535
51	3	99.46	1.34	11.83	3	1769.985
52	2	93.61	1.1	21.61	6	1616.626
54	4	98.96	1.25	21.8	6	1630.84
55	4	118.47	1.02	33.1	9	1650.789
56	3	118.49	1.08	11.88	3	1777.466
57	4	118.67	1.16	12.01	3	1796.916
58	4	118.34	1.17	12.06	3	1804.397
59	4	117.67	1.18	12.18	3	1822.352
60	3	104.48	1.35	12.14	3	1816.367
61	3	108.23	1.42	12.32	3	1843.298
62	2	105.1	1.38	12.05	3	1802.901
63	2	113.98	1.25	12.12	3	1813.374
64	2	113.89	1.25	12.16	3	1819.359
65	1	113.65	1.25	12.22	3	1828.336
66	1	113.83	1.25	12.24	3	1831.329
67	1	113.54	1.25	12.11	3	1811.878
76		104.75	1.7	17.75	5	1593.435
77		105.42	1.42	34.2	4	3837.711
78	4	137.93	1.11	34.1	8	1913.245
79	2	136.86	1.05	33.8	8	1896.413
80	2	135.31	0.99	33.5	8	1879.581
82	2	125.77	1.19	32.7	8	1834.695
84	2	123.31	0.7	30.8	8	1728.092
85	2	123.83	0.76	30.9	8	1733.703
86	2	126.32	1.01	33.3	8	1868.359

87	2	126.79	1.05	32.8	8	1840.306
88	2	123.39	1.31	30.2	8	1694.428
89	2	110.14	1.32	30.8	8	1728.092
94	2	235.59	0.82	33.2	8	1862.748
95	2	225.61	0.81	32.9	8	1845.916
96	2	162.29	1.1	33.4	8	1873.97
110	3	65.5	2.23	5.51	1	2473.191
111	3	62.53	1.81	10.8	3	1615.878
113	3	65.13	1.48	9.1	2	2042.29
121	2	66.38	1.73	9.5	2	2132.061
123	2	76.31	1.15	9.5	2	2132.061
124	2	68.31	1.15	11.5	3	1720.611
134	3	98.52	1.25	11.86	3	1774.474
137	3	110.4	0.79	31.49	8	1766.806
138	3	92.59	0.96	20.65	5	1853.771
142	3	89.54	0.96	16.3	4	1829.084
145	3	86.37	0.88	13.5	4	1514.886
148	3	87.68	0.93	16.44	4	1844.794
151	1	92.12	0.87	16.4	4	1840.306
210	2	91.85	1.82	17.2	4	1930.077
211	2	91.24	1.76	17.2	4	1930.077
213	2	95.27	1.64	17.9	4	2008.626
214	2	95.65	1.62	17.2	4	1930.077
218	2	82.24	1.73	17	4	1907.634
220		86.42	1.53	16.6	5	1490.199
225	2	91.76	1.36	15	4	1683.206
226	2	97.17	1.23	14.61	4	1639.443
227	2	100.8	1.15	14.35	4	1610.267
229	2	77.23	1.32	12.4	3	1855.268
230	2	76.63	1.28	12.2	3	1825.344
231	2	79.43	1.15	12	3	1795.42
232	2	79.73	1.13	12.02	3	1798.413
236	2	54.84	1.33	12	3	1795.42
246	2	62.01	1.04	11.4	3	1705.649
247	2	62.56	1.05	11.63	3	1740.061
248	2	58.52	1.13	12.3	3	1840.306
251	2	61.55	1.02	11.4	3	1705.649
252	2	58.05	1.27	11.9	3	1780.458
253	2	58.53	1.15	12	3	1795.42
254	2	64.5	0.99	11.7	3	1750.535
257	2	56.67	1.19	11.4	3	1705.649

258	2	54.09	1.18	11.8	3	1765.497
259	2	53.78	1.24	11.8	3	1765.497
260	2	51.58	1.27	11.8	3	1765.497
262	2	45.53	1.47	9	2	2019.848
263	2	46.87	1.47	9	2	2019.848
264	2	47.94	1.42	8.8	2	1974.962
265	2	50.94	1.08	11.48	3	1717.619
266	2	42.6	1.4	8.6	2	1930.077
267	2	36.65	1.37	8.6	2	1930.077
268	2	36.38	1.33	8.34	2	1871.726
269	2	27.98	1.19	4.6	1	2064.733
281		59.04	1.44	7.7	2	1728.092
282	2	57.96	1.42	12.3	3	1840.306
284	2	38.96	0.85	9.49	2	2129.817
285	2	25.48	1.31	4.6	1	2064.733
291	2	25.7	1.22	4.46	1	2001.894
292	2	25.29	1.3	4.6	1	2064.733